


96 GeV diphoton excess in seesaw extensions of the natural NMSSMJunjie Cao^{✉,*}, Xinglong Jia,[‡] Yuanfang Yue^{✉,§}, Haijing Zhou^{✉,†}, and Pengxuan Zhu^{✉,||}
Department of Physics, Henan Normal University, Xinxiang 453007, China (Received 4 October 2019; accepted 11 February 2020; published 5 March 2020)

The next-to minimal supersymmetric Standard Model (NMSSM) with a Type-I seesaw mechanism extends the NMSSM by three generations of right-handed neutrino fields to generate neutrino mass. As a byproduct, it renders the lightest sneutrino as a viable dark matter (DM) candidate. Due to the gauge singlet nature of the DM, its scattering with nucleon is suppressed in most cases to coincide spontaneously with the latest XENON-1T results. Consequently, broad parameter spaces in the Higgs sector, especially a light Higgsino mass, are resurrected as experimentally allowed, which makes the theory well suited to explain the long-standing $b\bar{b}$ excess at LEP-II and the continuously observed $\gamma\gamma$ excess by CMS Collaboration. We show by both analytic formulas and numerical results that the theory can naturally predict the central values of the excesses in its broad parameter space, and the explanations are consistent with the Higgs data of the discovered Higgs boson, B -physics, and DM physics measurements, the electroweak precision data, as well as the LHC search for sparticles. Part of the explanations may be tested by future DM experiments and the supersymmetry (SUSY) search at the LHC.

DOI: [10.1103/PhysRevD.101.055008](https://doi.org/10.1103/PhysRevD.101.055008)**I. INTRODUCTION**

Electroweak symmetry breaking (EWSB) is one of the most important issues in particle physics. The discovery of a Standard Model (SM)-like Higgs boson at the Large Hadron Collider (LHC) [1,2] indicates the correctness of Higgs mechanism, while the quadratically divergent correction to the boson mass in the SM implies the need of a more complex theoretical structure to account for the EWSB in a natural way. Without considering extreme cases, the complete EWSB mechanism should manifest itself by potentially sizable deviations (less than roughly 20% at 95% confidence level according to current Higgs data at the LHC [3]) of the boson's property from its SM prediction, and/or by exotic signals at colliders. Interestingly, so far it seems that the latter has emerged through a 2.3σ local excess for the channel $e^+e^- \rightarrow Z\phi_{b\bar{b}} \rightarrow Zb\bar{b}$ at LEP-II with the scalar mass $m_{\phi_{b\bar{b}}} \sim 98$ GeV [4,5] and also through a roughly 3σ local excess for the channel $pp \rightarrow \phi_{\gamma\gamma} \rightarrow \gamma\gamma$ at the LHC with

$m_{\phi_{\gamma\gamma}} \simeq 96$ GeV, which was reported recently by CMS Collaboration after combining 8 and 13 TeV data [6,7].¹ The normalized signal strengths of the excesses are [6,10]

$$\mu_{\text{LEP}} = \frac{\sigma(e^+e^- \rightarrow Z\phi_{b\bar{b}} \rightarrow Zb\bar{b})}{\sigma_{\text{SM}}(e^+e^- \rightarrow ZH_{\text{SM}} \rightarrow Zb\bar{b})} = 0.117 \pm 0.057, \quad (1.1)$$

$$\mu_{\text{CMS}} = \frac{\sigma(pp \rightarrow \phi_{\gamma\gamma} \rightarrow \gamma\gamma)}{\sigma_{\text{SM}}(pp \rightarrow H_{\text{SM}} \rightarrow \gamma\gamma)} = 0.6 \pm 0.2. \quad (1.2)$$

Since the mass resolution for the $b\bar{b}$ final state at LEP-II is rather coarse [9] and at same time $\phi_{b\bar{b}}$ and $\phi_{\gamma\gamma}$ are so close in mass, it is conjectured that the two excesses do not emerge accidentally and may have the same physical origin. So far, a variety of beyond SM theories were studied to reveal it, where the intermediate scalar ϕ is usually taken as a gauge singlet charge-parity (CP)-even Higgs or a singlet-like particle. These theories include the radion model [11,12], the singlet extensions of the SM by additional

*Corresponding author.
junjiecao@alumni.itp.ac.cn
†zhouhaijing0622@163.com
‡645665975@qq.com
§yuanfang405@gmail.com
||zhupx99@icloud.com

Published by the American Physical Society under the terms of the [Creative Commons Attribution 4.0 International license](https://creativecommons.org/licenses/by/4.0/). Further distribution of this work must maintain attribution to the author(s) and the published article's title, journal citation, and DOI. Funded by SCOAP³.

¹We note that the ATLAS Collaboration also published its analysis of about 80 fb^{-1} data on the diphoton signal [8], and it claims no significant excess over the SM expectation for the diphoton mass between 65 and 110 GeV. This result does not conflict with the CMS observation since the limit of the ATLAS analysis on the signal strength is significantly weaker than the corresponding one obtained by CMS Collaboration (see the comparison of the two limits in Fig. 1 of Ref. [9]). We infer from the two experimental reports that the low performance of the ATLAS analysis is mainly due to its relatively large uncertainties in determining the diphoton invariant mass $\phi_{\gamma\gamma}$ (see Fig. 2 of [8] and Fig. 1 of [7]) and also in fitting the continuum background of the signal.

vectorlike matter fields [13,14], the fermiophobic Type-I two Higgs doublet model (2HDM) [13,15], the singlet extensions of the 2HDM [16,17] and its supersymmetric version [namely the next-to-minimal supersymmetric Standard Model (NMSSM)] [9,10,18–22], as well as the μ -from- ν supersymmetric Standard Model [23,24]. Among these models, the NMSSM [25] is of particular interest because, due to the introduction of one singlet Higgs field, it has theoretical advantages over the popular minimal supersymmetric Standard Model (MSSM), such as generating dynamically the μ term, which is responsible for Higgsino mass, and providing more feasible dark matter (DM) candidates so that the model's phenomenology is enriched greatly [26–29]. Moreover, as far as the light CP -even Higgs scenario of the model (which is appropriate to explain the excesses) is concerned, the mass of the SM-like Higgs boson can be significantly lifted up by both an additional tree-level contribution and the singlet-doublet mixing effect [30–32], which makes large radiative corrections from stop loops unnecessary in predicting $m_h \simeq 125$ GeV, and the Higgsino mass is upper bounded by about 400 GeV, which is the right range to predict Z boson mass in a natural way [31,33,34].

A thorough analysis of the light Higgs scenario in the general NMSSM was recently performed in [22] by both compact analytic formulas and numerical results. It was concluded that there are parameter spaces where the excesses can be well explained without conflicting with the 125 GeV Higgs data collected at the LHC. With regard to such a study, we remind that for the NMSSM as one of the most intensively studied supersymmetric theories, its parameter space in Higgs sector has been tightly limited by DM physics and also by the LHC search for sparticles [35], which should be considered in a comprehensive study of the excesses. The tightness of the constraints comes from the following facts:

- (i) In the NMSSM, the lightest neutralino (usually with Bino or Singlino field as its dominant component) is customarily taken as a DM candidate. Some parameters in the neutralino sector of the theory, such as λ , κ , $\tan\beta$, and μ , are also inputs of the Higgs sector [25]. Notably, besides affecting the Higgs mass spectrum, these parameters usually play an important role in determining the DM property, such as its mass, field component, as well as interactions with Higgs and SM gauge bosons [36]. So, they are restricted by the measurements in DM physics.
- (ii) Given that squarks and sleptons are preferred heavy by the direct search for sparticles at the LHC and consequently they have little effect on DM physics when $m_{\text{DM}} \sim 100$ GeV, the Higgs bosons and the SM gauge bosons often act as the mediators or final states of DM annihilation. Then the DM relic density precisely measured by WMAP and Planck experiments [37] requires fine-tuned configurations of the involved parameters [36,38].

- (iii) So far, XENON-1T experiment has reached unprecedented sensitivity in detecting DM-nucleon scattering, i.e., $\sigma^{\text{SI}} \sim 10^{-47}$ cm² for spin-independent (SI) cross section [39] and $\sigma^{\text{SD}} \sim 10^{-41}$ cm² for spin-dependent (SD) cross section [40]. Since the t-channel exchange of Higgs bosons (Z boson) is the dominant contribution to the SI (SD) cross section at tree level, the experiment can exclude a large portion of the parameter space in the Higgs sector, especially in case of light Higgsinos and/or light Higgs bosons where strong cancellation between different Higgs contributions must be present to coincide with the experimental results [41,42].
- (iv) With the smooth progress of the LHC in looking for electroweakinos by multilepton signals, the mass spectrum of neutralinos and charginos has been tightly limited within certain patterns for $\mu \lesssim 500$ GeV [35].

In fact, we once studied the excesses in the NMSSM with a \mathbb{Z}_3 discrete symmetry by considering the constraints from LUX and PandaX experiments on the DM-nucleon scattering in 2016. We found that they can be explained at 1σ level only in a very narrow parameter space and at the cost of relaxing the relic density constraint [10]. Since the latest XENON-1T results have improved the previous sensitivity by a factor of about 5, we checked that the space becomes experimentally disfavored [35].

Given the great theoretical advantages of the NMSSM and unfortunately the strong experimental constraints on its most natural parameter space, we were motivated to augment the NMSSM with different seesaw mechanisms to generate neutrino mass and also to enable the lightest sneutrino $\tilde{\nu}_1$ as a viable DM candidate [43–46]. The general feature of such extensions is that the singlet Higgs field plays extra roles [43,44]: apart from being responsible for heavy neutrino mass via the interaction $\hat{S}\hat{\nu}\hat{\nu}$ in superpotential (\hat{S} and $\hat{\nu}$ denote the superfields of the singlet Higgs and the heavy neutrino, respectively), it contributes to the annihilation of $\tilde{\nu}_1$ and consequently makes the property of $\tilde{\nu}_1$ compatible with various measurements in a natural way. This can be understood from two popular cases. One is that the singlet Higgs can mediate the transition between the $\tilde{\nu}_1$ pair and the Higgsino pair so that $\tilde{\nu}_1$ and the Higgsinos are in thermal equilibrium in early universe before their freeze-out. If their mass splitting is less than about 10%, the number density of the Higgsinos can track that of $\tilde{\nu}_1$ during freeze-out, and as a result the Higgsinos played a dominant role in determining the density due to its relatively strong interaction with SM particles [47] (in literature such a phenomenon was called coannihilation [48]). In this case, the constraint on the Higgsino mass μ from the LHC search for electroweakinos is rather weak due to the compressed spectrum, and light Higgsinos with $\mu \sim 100$ GeV are still allowed. The other is that, due to its gauge singlet nature, $\tilde{\nu}_1$ and the singlet Higgs

can compose a secluded DM sector where the measured relic abundance can be accounted for by the annihilation of $\tilde{\nu}_1$ into a pair of the singlet Higgs. In both the cases, $\tilde{\nu}_1$ couples very weakly with the SM particles so that its scattering with nucleon is always suppressed, which is consistent with current DM direct detection (DD) results. This is a great theoretical advantage in light of the tight experimental limit. At this stage, we emphasize that, when one fixes the mass spectrum of the Higgs bosons and neutralinos, it usually happens that the theory is kept compatible with various DM measurements only by adjusting the parameters in the sneutrino sector [43–45]. This reflects the fact that, although the DM sector and the Higgs sector of the theory are entangled together to survive various experimental constraints, which is the same as the NMSSM, their correlation becomes loose and the constraints from DM physics are weakened greatly. This will resurrect broad parameter spaces in the Higgs sector as experimentally allowed and thus make the theory suitable to explain the excesses. This feature was not noticed in the previous works [43–45], and studying the capability of the augmented theory to explain the excesses is the main aim of this work.

This paper is organized as follows. In Sec. II, we first take the NMSSM with a Type-I seesaw mechanism (Type-I NMSSM) as an example to recapitulate the basics of the more general framework where the NMSSM is augmented by different seesaw mechanisms, including its field content and Lagrangian, then we turn to discuss the conditions to produce sizable $b\bar{b}$ and $\gamma\gamma$ signals. In Sec. III, we perform a comprehensive scan over the vast parameter space of the Higgs sector to look for the regions where the excesses can be well explained. In this process, we consider some experimental results, such as the Higgs data of the discovered Higgs, B -physics measurements, as well as precision electroweak measurements, to limit the parameter space, and plot the map of the profile likelihood (PL) for the excesses on different planes to study their implication in the theory. In Sec. IV, we further study the constraints from the DM physics and the sparticle search, and point out that some explanations can easily survive the constraints. We also choose one parameter point to show that the fine-tunings associated with the excesses are not serious. Conclusions are made in Sec. V.

II. THEORETICAL PRELIMINARIES

A. NMSSM with the Type-I seesaw mechanism

As the simplest extension of the NMSSM, the Type-I NMSSM augments the NMSSM by three generation right-handed neutrino fields to generate neutrino masses. With the field content presented in Table I, its superpotential W and soft breaking terms L_{soft} are [49,50]

TABLE I. Field content of the NMSSM with Type-I seesaw mechanism.

Superfield	Spin 0	Spin $\frac{1}{2}$	Generations	$(U(1) \otimes SU(2) \otimes SU(3))$
\hat{q}	\tilde{q}	q	3	$(\frac{1}{6}, \mathbf{2}, \mathbf{3})$
\hat{l}	\tilde{l}	l	3	$(-\frac{1}{2}, \mathbf{2}, \mathbf{1})$
\hat{H}_d	H_d	\tilde{H}_d	1	$(-\frac{1}{2}, \mathbf{2}, \mathbf{1})$
\hat{H}_u	H_u	\tilde{H}_u	1	$(\frac{1}{2}, \mathbf{2}, \mathbf{1})$
\hat{d}	\tilde{d}_R^*	d_R^*	3	$(\frac{1}{3}, \mathbf{1}, \bar{\mathbf{3}})$
\hat{u}	\tilde{u}_R^*	u_R^*	3	$(-\frac{2}{3}, \mathbf{1}, \bar{\mathbf{3}})$
\hat{e}	\tilde{e}_R^*	e_R^*	3	$(1, \mathbf{1}, \mathbf{1})$
\hat{s}	S	\tilde{S}	1	$(0, \mathbf{1}, \mathbf{1})$
$\hat{\nu}$	$\tilde{\nu}_R^*$	ν_R^*	3	$(0, \mathbf{1}, \mathbf{1})$

$$\begin{aligned}
W &= W_F + \lambda \hat{s} \hat{H}_u \cdot \hat{H}_d + \frac{1}{3} \kappa \hat{s}^3 + \bar{\lambda}_\nu \hat{s} \hat{\nu} \hat{\nu} + Y_\nu \hat{l} \cdot \hat{H}_u \hat{\nu}, \\
L_{\text{soft}} &= m_{H_d}^2 |H_d|^2 + m_{H_u}^2 |H_u|^2 + m_S^2 |S|^2 + \bar{m}_{\tilde{\nu}_R}^2 \tilde{\nu}_R^* \\
&\quad + (\lambda A_\lambda S H_u \cdot H_d + \frac{1}{3} \kappa A_\kappa S^3 + \bar{\lambda}_\nu \bar{A}_{\lambda_\nu} S \tilde{\nu}_R^* \tilde{\nu}_R^* \\
&\quad + Y_\nu \bar{A}_\nu \tilde{\nu}_R^* \tilde{H}_u + \text{H.c.}) + \dots, \tag{2.1}
\end{aligned}$$

where W_F denotes the superpotential of the MSSM without the μ term, and a \mathbb{Z}_3 symmetry is considered to forbid the appearance of any dimensional parameters in W . The coefficients λ and κ parametrize the interactions among the Higgs fields, and Y_ν and $\bar{\lambda}_\nu$ are neutrino Yukawa couplings with flavor index omitted to make the formulas concise and more intuitive. Since the soft breaking squared masses $m_{H_u}^2$, $m_{H_d}^2$, and m_S^2 are related with the vacuum expectation values of the fields H_u , H_d , and S , $\langle H_u \rangle = v_u/\sqrt{2}$, $\langle H_d \rangle = v_d/\sqrt{2}$, and $\langle S \rangle = v_s/\sqrt{2}$, by the minimization conditions of the Higgs potential after the electroweak symmetry breaking [25], it is customary to take λ , κ , $\tan \beta \equiv v_u/v_d$, A_λ , A_κ , and $\mu \equiv \lambda v_s/\sqrt{2}$ as theoretical input parameters of the Higgs sector.

Same as the NMSSM, one usually introduces following combinations of the Higgs fields:

$$\begin{aligned}
H_1 &= \cos \beta H_u + \varepsilon \sin \beta H_d^*, & H_2 &= \sin \beta H_u - \varepsilon \cos \beta H_d^*, \\
H_3 &= S, \tag{2.2}
\end{aligned}$$

where ε is two-dimensional antisymmetric tensor, i.e., $\varepsilon_{12} = -\varepsilon_{21} = 1$ and $\varepsilon_{11} = \varepsilon_{22} = 0$. In this representation, H_i ($i = 1, 2, 3$) take the following form:

$$\begin{aligned}
H_1 &= \begin{pmatrix} H^+ \\ \frac{S_1 + iP_1}{\sqrt{2}} \end{pmatrix}, & H_2 &= \begin{pmatrix} G^+ \\ v + \frac{S_2 + iG^0}{\sqrt{2}} \end{pmatrix}, \\
H_3 &= v_s + \frac{1}{\sqrt{2}} (S_3 + iP_2). \tag{2.3}
\end{aligned}$$

These expressions indicate that the field H_2 corresponds to the SM Higgs field, and the fields S_1 , S_2 , and S_3 mix to

form three physical CP -even Higgs bosons. Therefore, the CP -even Higgs boson with largest S_2 component is called the SM-like Higgs boson. In the basis (S_1, S_2, S_3) , the mass matrix is given by [31]

$$\begin{aligned} M_{11}^2 &= \frac{2\mu(\lambda A_\lambda + \kappa\mu)}{\lambda \sin 2\beta} + \left(m_Z^2 - \frac{1}{2}\lambda^2 v^2\right) \sin^2 2\beta \\ M_{12}^2 &= -\frac{1}{4}(2m_Z^2 - \lambda^2 v^2) \sin 4\beta \\ M_{13}^2 &= -\sqrt{2}(\lambda A_\lambda + 2\kappa\mu) v \cos 2\beta \\ M_{22}^2 &= m_Z^2 \cos^2 2\beta + \frac{1}{2}\lambda^2 v^2 \sin^2 2\beta \\ M_{23}^2 &= \frac{v}{\sqrt{2}}[2\lambda\mu - (\lambda A_\lambda + 2\kappa\mu) \sin 2\beta] \\ M_{33}^2 &= \frac{\lambda^2 v^2 A_\lambda \sin 2\beta}{4\mu} + \frac{\mu}{\lambda} \left(\kappa A_\kappa + 4\kappa^2 \frac{\mu}{\lambda}\right), \end{aligned} \quad (2.4)$$

where the expression of M_{22}^2 indicates that the SM Higgs mass at tree level gets an additional contribution $\frac{1}{2}\lambda^2 v^2 \sin^2 2\beta$ in comparison with corresponding MSSM prediction. The matrix also indicates that if the relation $M_{33}^2 < m_{22}^2$ holds, the mixing between the fields S_2 and S_3 can further enhance the mass of the S_2 -dominated state. Benefiting from the contributions, the SM-like Higgs boson does not need a large radiative contribution from stop loops to get its mass around 125 GeV [30–32]. Due to the attractive feature, this case was called natural NMSSM in literature [51]. The model also predicts two CP -odd mass eigenstates A_i ($i = 1, 2$), which are the mixtures of the fields P_1 and P_2 , and a pair of charged Higgs bosons $H^\pm = \cos\beta H_u^\pm + \sin\beta H_d^\pm$. Throughout this paper, we label the neutral eigenstates in an ascending mass order, i.e., $m_{h_1} < m_{h_2} < m_{h_3}$ and $m_{A_1} < m_{A_2}$.

The Higgs sector of the model has the following features:

- (i) One CP -even state corresponds to the Higgs boson discovered at the LHC. Since experimental measurements require its property quite SM Higgs-like, the mixing of the S_2 field with the other fields should be less than about 10% [3]. This implies from the definition of the S_1 and S_2 fields that it is $\text{Re}[H_u^0]$ dominated if $\tan\beta \gg 1$, and the heavy doublet-dominated state is mainly composed by $\text{Re}[H_d^0]$.
- (ii) Similar to the situation of the MSSM, the heavy doublet-dominated CP -even state is roughly degenerate in mass with the doublet-dominated CP -odd state and also with the charged states. The LHC search for extra Higgs bosons together with the indirect constraints from B -physics has required $m_{H^\pm} \gtrsim 0.5$ TeV [52].
- (iii) With regard to the singlet-dominated states, they may be very light without conflicting with relevant collider constraints. One new function of these states is that they can couple directly with the sneutrino

pair by three and four scalar interactions, which are induced by the $\bar{\lambda}_\nu \hat{s} \hat{\nu} \hat{\nu}$ term in the superpotential and its soft breaking term. As a result, they may appear as the final state of the sneutrino pair annihilation in early universe or mediate the annihilation and thus play an important role in sneutrino DM physics.

In the following, we recapitulate the features of the neutrino and sneutrino sectors in the Type-I NMSSM, which differ greatly from those of the NMSSM. We first focus on the neutrino sector. The neutrino Yukawa interactions take the following form:

$$\mathcal{L}_\nu = \nu_R^* Y_\nu H_u^0 \nu_L + \nu_R^* \bar{\lambda}_\nu S \nu_R^* + \text{H.c.}, \quad (2.5)$$

and they are responsible for neutrino masses after the involved Higgs fields develop vevs. In the interaction basis (ν_L, ν_R^*) , the 6×6 neutrino mass matrix reads

$$M_{\text{Type-I}} = \begin{pmatrix} 0 & \frac{v_u}{\sqrt{2}} Y_\nu \\ \frac{v_u}{\sqrt{2}} Y_\nu^T & \sqrt{2} v_s \bar{\lambda}_\nu \end{pmatrix}, \quad (2.6)$$

and given that the magnitude of the right-handed neutrino mass matrix $M = \sqrt{2} v_s \bar{\lambda}_\nu$ is much larger than that of $\frac{v_u}{\sqrt{2}} Y_\nu$, the heavy fields can be integrated out to get the 3×3 mass matrix of light active neutrinos [53], $M_\nu = \frac{1}{2} Y_\nu v_u M^{-1} Y_\nu^T v_u$. This symmetric effective mass matrix can be diagonalized by the unitary Pontecorvo-Maki-Nakagawa-Sakata (PMNS) matrix as follows:

$$U_{\text{PMNS}}^T M_\nu U_{\text{PMNS}} = \text{diag}(m_{\nu_1}, m_{\nu_2}, m_{\nu_3}), \quad (2.7)$$

with m_{ν_1} , m_{ν_2} , and m_{ν_3} denoting the masses of the three lightest neutrinos. Since the PMNS matrix has been determined by neutrino experiments (especially by neutrino oscillation data) [54], one can express the Yukawa coupling matrix Y_ν in terms of the U_{PMNS} by a modified Casas-Ibarra parametrization [55],

$$\begin{aligned} \frac{v_u}{\sqrt{2}} Y_\nu^T &= V^\dagger \text{diag}(\sqrt{M_1}, \sqrt{M_2}, \sqrt{M_3}) \\ &\times R \text{diag}(\sqrt{m_{\nu_1}}, \sqrt{m_{\nu_2}}, \sqrt{m_{\nu_3}}) U_{\text{PMNS}}^\dagger, \end{aligned} \quad (2.8)$$

where V is a unitary matrix that diagonalizes M by $M = V^\dagger \text{diag}(M_1, M_2, M_3) V^*$, and R is a complex orthogonal matrix given by

$$R = \begin{pmatrix} c_2 c_3 & -c_1 s_3 - s_1 s_2 c_3 & s_1 s_3 - c_1 s_2 c_3 \\ c_2 s_3 & c_1 c_3 - s_1 s_2 s_3 & -s_1 c_3 - c_1 s_2 s_3 \\ s_2 & s_1 c_2 & c_1 c_2 \end{pmatrix}, \quad (2.9)$$

with $c_i \equiv \cos \theta_i$, $s_i \equiv \sin \theta_i$ and θ_1 , θ_2 , and θ_3 being arbitrary angles. This formula shows that the neutrino Yukawa coupling Y_ν is generally flavor nondiagonal, and

for $m_{\nu_i} \sim 0.1$ eV indicated by neutrino experiments and $M_i \sim \mathcal{O}(100 \text{ GeV})$ by our setting, the magnitude of its elements is at the order of 10^{-6} .

Next, we consider the sneutrino sector of the extension. One particular feature about the sneutrinos is that the lightest $\tilde{\nu}_R$ -dominated sneutrino can act as a viable DM candidate,² and the advantage of such a choice over the customary neutralino DM is that, if v_s is not excessively large (e.g., less than several TeV), the couplings of the sneutrino pair with SM particles are always weak due to its singlet nature. This causes its scattering with nucleon to be suppressed greatly and thus alleviates the constraints of the DM DD experiments on the theory [44]. Throughout this work, we only discuss the case with a sneutrino DM since it corresponds to much broader parameter space allowed by current experiments.

For the neutrino/sneutrino sector, if one resorts the neutrino oscillations solely to the non-diagonality of the Yukawa coupling Y_ν , $\bar{\lambda}_\nu$ is flavor diagonal. If one further takes the soft breaking parameters \bar{m}_τ (slepton soft breaking mass), $\bar{m}_{\tilde{\nu}}$, \bar{A}_{λ_ν} , and \bar{A}_ν to be flavor diagonal, the flavor mixings of the sneutrinos are extremely suppressed by the off-diagonal elements of Y_ν , and it is a good approximation to only consider one generation sneutrinos in studying the properties of the sneutrino DM [44]. In our discussion, we assume the sneutrino DM carrying a τ flavor, which is motivated by the fact that in some fundamental supersymmetric theories with supersymmetry broken at a high energy scale by certain mechanisms, the third generation sfermions are usually lighter than the other generation ones due to the renormalization group effects.³ As a result, the parameters of the first two generation sneutrinos are irrelevant to our discussion. We use the symbols $m_{\tilde{\nu}}$, λ_ν , A_{λ_ν} , and $m_{\tilde{\nu}}$ to denote the 33 elements of the matrix \bar{m}_τ , $\bar{\lambda}_\nu$, \bar{A}_{λ_ν} , and $\bar{m}_{\tilde{\nu}}$, respectively and treat all these parameters as real numbers. Then after decomposing the sneutrino field into CP -even and CP -odd parts,

$$\tilde{\nu}_L \equiv \frac{1}{\sqrt{2}}(\tilde{\nu}_{L1} + i\tilde{\nu}_{L2}), \quad \tilde{\nu}_R \equiv \frac{1}{\sqrt{2}}(\tilde{\nu}_{R1} + i\tilde{\nu}_{R2}), \quad (2.10)$$

²Note that although the $\bar{\lambda}_\nu \hat{s} \hat{\nu} \hat{\nu}$ term in the superpotential violates lepton number by $\Delta L = 2$, it does not spoil R -parity, which is defined by $R \equiv (-1)^{3B+L+2S}$ with B , L , and S denoting baryon number, lepton number, and spin of the involved field, respectively, since ΔL is an even number. One can check this conclusion by studying the interactions induced by the term.

³From the perspective of collider phenomenology, the hypothesis predicts that charged supersymmetric particles decay ultimately into τ leptons in some popular cases. Detecting such a signal at the LHC is more difficult than the signal containing electrons or muon leptons, which can be learnt from the latest search for sleptons at the LHC (see [56] for $\tilde{\nu}_{L,R}/\tilde{\mu}_{L,R}$ and [57] for $\tilde{\tau}_{L,R}$, as well as [58,59] for compressed sparticle spectrum case). This makes the extension readily consistent with the results of the LHC in searching for supersymmetry.

the sneutrino mass terms are written as [44]

$$\frac{1}{2}(\tilde{\nu}_{Li}, \tilde{\nu}_{Ri}) \begin{pmatrix} m_{L\bar{L}}^2 & \pm m_{LR}^2 + m_{L\bar{R}}^2 \\ \pm m_{LR}^2 + m_{L\bar{R}}^2 & m_{R\bar{R}}^2 \pm 2m_{RR}^2 \end{pmatrix} \begin{pmatrix} \tilde{\nu}_{Li} \\ \tilde{\nu}_{Ri} \end{pmatrix}, \quad (2.11)$$

where $i = 1, 2$ denote different CP states, the minus signs in the matrix are for the CP -odd states, and

$$\begin{aligned} m_{L\bar{L}}^2 &\equiv m_{\tilde{l}}^2 + |Y_\nu v_u|^2 + \frac{1}{8}(g_1^2 + g_2^2)(v_d^2 - v_u^2), \\ m_{LR}^2 &\equiv 2Y_\nu v_u (\lambda v_s)^*, \\ m_{L\bar{R}}^2 &\equiv Y_\nu (-\lambda v_s v_d)^* + Y_\nu A_{Y_\nu} v_u, \\ m_{R\bar{R}}^2 &\equiv m_{\tilde{\nu}}^2 + |2\lambda_\nu v_s|^2 + |Y_\nu v_u|^2, \\ m_{RR}^2 &\equiv \lambda_\nu (A_{\lambda_\nu} v_s + (\kappa v_s^2 - \lambda v_d v_u)^*). \end{aligned} \quad (2.12)$$

Equation (2.11) indicates that the chiral mixings of the sneutrino fields are proportional to Y_ν , and hence can be ignored safely. So the sneutrino mass eigenstate coincides with the chiral state. It also indicates that, due to the presence of lepton number violating interactions in the superpotential, the CP -even and -odd components of the right-handed sneutrino field are usually not degenerate in mass, and consequently the sneutrino DM has a definite CP number. For more discussion about the property of the sneutrino DM, one can see our previous work [44].

Possible annihilation channels of the sneutrino DM include [49,50] the following:

- (1) $\tilde{\nu}_1 \tilde{H} \rightarrow XY$ and $\tilde{H} \tilde{H}' \rightarrow X'Y'$ with \tilde{H} and \tilde{H}' denoting any Higgsino-dominated neutralino or chargino and $X^{(\prime)}$ and $Y^{(\prime)}$ representing any lighter state. These annihilation channels are called coannihilation in literature [47,48], and they are important only when the mass splitting between \tilde{H} and $\tilde{\nu}_1$ is less than about 10%. As pointed out by the Bayesian analysis of the model in [44], this channel is the most important annihilation mode.
- (2) $\tilde{\nu}_1 \tilde{\nu}_1 \rightarrow ss^*$ via the s -channel exchange of a Higgs boson, the t/u -channel exchange of a sneutrino, and any relevant scalar quartic couplings with s denoting a light Higgs boson. This is the second important annihilation channel of the DM.
- (3) $\tilde{\nu}_1 \tilde{\nu}_1 \rightarrow VV^*$, Vs , $f\bar{f}$ with V and f denoting a vector boson (W or Z) and a SM fermion, respectively. This kind of annihilations proceeds via the s -channel exchange of a CP -even Higgs boson.
- (4) $\tilde{\nu}_1 \tilde{\nu}_1 \rightarrow \nu_R \bar{\nu}_R$ via the s -channel exchange of a Higgs boson and the t/u -channel exchange of a neutralino.
- (5) $\tilde{\nu}_1 \tilde{\nu}'_1 \rightarrow A_i^{(*)} \rightarrow XY$ and $\tilde{\nu}'_1 \tilde{\nu}'_1 \rightarrow X'Y'$ with $\tilde{\nu}'_1$ denoting a sneutrino with an opposite CP number to that of $\tilde{\nu}_1$. These annihilation channels are important in determining the relic density only when the CP -even and -odd states are nearly degenerate in mass.

The expressions of σv for some channels are presented in [50]. One can learn from them that the parameters in sneutrino sector, such as λ_ν , A_ν , and $m_{\tilde{\nu}}^2$, as well as the parameters in the Higgs sector, are involved in the annihilations.

Note that the above introduction reveals the fact that the singlet Higgs field in the seesaw extension of the NMSSM plays an important roles in both Higgs physics and DM physics, e.g., besides being responsible for μ term and affecting Higgs mass spectrum, it also accounts for right-handed neutrino masses and sneutrino DM annihilation. This feature makes the theory quite distinct from its corresponding extension of the MSSM.

B. Formula for the $b\bar{b}$ and $\gamma\gamma$ signals

In the seesaw extension of the NMSSM, the singlet-dominated CP -even h_1 may account for both excesses. In order to illustrate this point, let us first look at the analytic expression of the signal strengths for the excesses in the narrow width approximation. The diphoton signal strength normalized to its SM prediction is given by

$$\begin{aligned} \mu_{\text{CMS}}|_{m_{h_1} \simeq 96 \text{ GeV}} &= \frac{\sigma_{\text{SUSY}}(pp \rightarrow h_1)}{\sigma_{\text{SM}}(pp \rightarrow h_1)} \times \frac{\text{Br}_{\text{SUSY}}(h_1 \rightarrow \gamma\gamma)}{\text{Br}_{\text{SM}}(h_1 \rightarrow \gamma\gamma)} \\ &\simeq \frac{\sigma_{\text{SUSY,ggF}}(pp \rightarrow h_1)}{\sigma_{\text{SM,ggF}}(pp \rightarrow h_1)} \\ &\quad \times \frac{\Gamma_{\text{SUSY}}(h_1 \rightarrow \gamma\gamma)}{\Gamma_{\text{SUSY}}^{\text{tot}} \times \text{Br}_{\text{SM}}(h_1 \rightarrow \gamma\gamma)} \\ &\simeq |C_{h_1 gg}|^2 \times \frac{\Gamma_{\text{SUSY}}(h_1 \rightarrow \gamma\gamma)}{\Gamma_{\text{SUSY}}^{\text{tot}}} \\ &\quad \times \frac{1}{1.43 \times 10^{-3}}, \end{aligned} \quad (2.13)$$

where the mass of the Higgs boson h_1 (denoted by m_{h_1}) is fixed around 96 GeV, and the subscript SUSY (SM) denotes the predictions of the Type-I NMSSM (SM) on the inclusive production rate of h_1 , its decay branching ratio into $\gamma\gamma$ and its width, which are labeled as $\sigma(pp \rightarrow h_1)$, $\text{Br}(h_1 \rightarrow \gamma\gamma)$, and Γ , respectively. As shown in the experimental analysis [7], the production rate $\sigma(pp \rightarrow h_1)$ is mainly contributed by gluon fusion (ggF) process, vector boson fusion (VBF) process, vector boson associated production (VH), as well as $t\bar{t}h_1$ production. Among these contributions, the ggF process is the main one in the SM (which contributes about 86% of the signal [7]) and also in the Type-I NMSSM (see footnote 4 below), so we approximate $\sigma(pp \rightarrow h_1)$ in the first equation by $\sigma_{\text{ggF}}(pp \rightarrow h_1)$ in the second step of the formula. In the final expression, $C_{h_1 gg}$ represents the supersymmetry (SUSY) prediction of $h_1 gg$ coupling which is normalized to its SM prediction, and in the leading order approximation it is equal to the

ratio $\sigma_{\text{SUSY,ggF}}(pp \rightarrow h_1)/\sigma_{\text{SM,ggF}}(pp \rightarrow h_1)$.⁴ $\Gamma_{\text{SUSY}}^{\text{tot}} = \Gamma_{\text{SUSY}}(h_1 \rightarrow b\bar{b}) + \Gamma_{\text{SUSY}}(h_1 \rightarrow c\bar{c}) + \dots$ denotes the SUSY prediction on the total width of h_1 , and 1.43×10^{-3} corresponds to the branching ratio of $h_1 \rightarrow \gamma\gamma$ in the SM for $m_{h_1} = 96$ GeV, which includes all known higher-order QCD corrections and is calculated by LHC Higgs Cross Section Working Group [60]. In getting the value of μ_{CMS} by the final expression, we include all one-loop contributions (which are induced by quarks and squarks) to $C_{h_1 gg}$ and all leading order contributions to $\Gamma_{\text{SUSY}}(h_1 \rightarrow \gamma\gamma)$ and $\Gamma_{\text{SUSY}}^{\text{tot}}$. The signal strength of the $b\bar{b}$ excess, μ_{LEP} , is defined in a similar way to μ_{CMS} , and is given by

$$\begin{aligned} \mu_{\text{LEP}}|_{m_{h_1} \simeq 96 \text{ GeV}} &= \frac{\sigma_{\text{SUSY}}(e^+e^- \rightarrow Zh_1)}{\sigma_{\text{SM}}(e^+e^- \rightarrow Zh_1)} \times \frac{\text{Br}_{\text{SUSY}}(h_1 \rightarrow b\bar{b})}{\text{Br}_{\text{SM}}(h_1 \rightarrow b\bar{b})} \\ &= |C_{h_1 VV}|^2 \times \frac{\Gamma_{\text{SUSY}}(h_1 \rightarrow b\bar{b})}{\Gamma_{\text{SUSY}}^{\text{tot}}} \times \frac{1}{0.799}, \end{aligned} \quad (2.14)$$

where $C_{h_1 VV}$ is the normalized coupling of h_1 with vector bosons, and 0.799 is value of $\text{Br}(h_1 \rightarrow b\bar{b})$ in the SM presented by the Higgs Cross Section Working Group [60].

From the formulas of μ_{CMS} and μ_{LEP} , one can learn two facts. One is that both strengths are expressed in term of the ratio $\sigma_{\text{SUSY}}/\sigma_{\text{SM}}$, and consequently the QCD correction to the numerator and the denominator will cancel. This is beneficial to reduce the theoretical uncertainty in predicting the strengths. The other is that, in order to explain both excesses by a singlet Higgs boson, h_1 cannot be CP odd because a CP -odd Higgs boson does not couple with ZZ and consequently it has no contribution to the $b\bar{b}$ excess. If alternatively one just wants to explain the diphoton excess, the Higgs boson can be either CP -even or CP -odd.

Next, we scrutinize the involved couplings. Since current LHC data have required the properties of the discovered boson to highly mimic those of the SM Higgs boson and meanwhile colored sparticles heavier than about 1 TeV, we have the following approximation for the normalized couplings of h_1 [10]:

$$\begin{aligned} C_{h_1 t\bar{t}} &\simeq -V_{11} \cot \beta + V_{12}, & C_{h_1 gg} &\simeq C_{h_1 t\bar{t}}, \\ C_{h_1 b\bar{b}} &\simeq V_{11} \tan \beta + V_{12}, & C_{h_1 VV} &= V_{12}, \end{aligned} \quad (2.15)$$

⁴Note that since $C_{h_1 VV} \simeq C_{h_1 t\bar{t}} \simeq C_{h_1 gg}$ (see the following discussion), $\sigma_{\text{SUSY,ggF}}/\sigma_{\text{SM,ggF}} \simeq \sigma_{\text{SUSY,VBF}}/\sigma_{\text{SM,VBF}} \simeq \sigma_{\text{SUSY,VH}}/\sigma_{\text{SM,VH}} \simeq \sigma_{\text{SUSY},t\bar{t}h_1}/\sigma_{\text{SM},t\bar{t}h_1} \simeq C_{h_1 gg}$. This implies that the ggF process is still the dominant one in contributing to the cross section $\sigma(pp \rightarrow h_1)$ in the Type-I NMSSM, and $C_{h_1 gg}$ in the final expression of Eq. (2.13) can be treated as an approximation of the ratio $\sigma_{\text{SUSY}}(pp \rightarrow h_1)/\sigma_{\text{SM}}(pp \rightarrow h_1)$. The goodness of this approximation is not sensitive to the fraction of the ggF contribution to the total signal.

where V_{ij} with $i, j = 1, 2, 3$ denotes the element of the rotation matrix to diagonalize the mass matrix in Eq. (2.4). As for $C_{h_1\gamma\gamma}$, besides the top quark- and W-mediated loops, it is also contributed by chargino loops and charged Higgs loop, i.e., $C_{h_1\gamma\gamma} = C_{h_1\gamma\gamma}^t + C_{h_1\gamma\gamma}^{W^\pm} + C_{h_1\gamma\gamma}^{\tilde{\chi}^\pm} + C_{h_1\gamma\gamma}^{H^\pm}$. Although the charged Higgs loop is usually negligible since it is mediated by a heavy scalar particle [51], the Higgsino-dominated chargino loop may play a role in enhancing $\Gamma(h_1 \rightarrow \gamma\gamma)$, which can be inferred from [61]

$$\begin{aligned} C_{h_1\gamma\gamma}^{\tilde{\chi}^\pm} &\simeq \left(\frac{2}{9} A_{1/2}(\tau_t) - \frac{7}{8} A_1(\tau_W) \right)^{-1} \times \frac{\lambda v}{6|\mu|} \left(1 + \frac{7 m_{h_1}^2}{304\mu^2} \right) V_{13} \\ &\simeq -1.37 \times \frac{\lambda v}{6|\mu|} \left(1 + \frac{7 m_{h_1}^2}{304\mu^2} \right) V_{13} \quad \text{for } m_{h_1} = 96 \text{ GeV}, \end{aligned} \quad (2.16)$$

with $A_{1/2}$ and A_1 being loop functions with $\tau_i = m_i^2/(4m_t^2)$. For example, if $\lambda > \frac{1}{5.6V_{13}} \frac{|\mu|}{100 \text{ GeV}}$, one has $|C_{h_1\gamma\gamma}^{\tilde{\chi}^\pm}| \gtrsim 0.1$. This is not a negligible number since $C_{h_1\gamma\gamma} \simeq 0.3$ can account for the diphoton excess at 1σ level (see the results in Fig. 2).

From these formulas, one can learn the following facts:

- (i) If the theory is used to explain the excesses, the preferred mass spectrum is $m_{h_1} \simeq 96 \text{ GeV}$, $m_{h_2} \simeq 125 \text{ GeV}$, and $m_{h_3} \simeq m_{H^\pm} \gtrsim 500 \text{ GeV}$. Since the splitting between m_{h_1} and m_{h_3} is much larger than that between m_{h_1} and m_{h_2} , $V_{12} \gg V_{11}$ is valid for most cases. So one can conclude that $C_{h_1VV} \simeq C_{h_1\tilde{t}\tilde{t}} \simeq C_{h_1gg} \simeq V_{12}$ and $C_{h_1\gamma\gamma}^t + C_{h_1\gamma\gamma}^W \simeq V_{12}$. This estimation is helpful to understand the strengths.
- (ii) $C_{h_1b\bar{b}}$ may be significantly smaller than $C_{h_1\tilde{t}\tilde{t}}$ due to the cancellation between $V_{11} \tan\beta$ and V_{12} . In this case, $\Gamma_{\text{SUSY}}^{\text{tot}}$ is reduced greatly, but it does not change the fact that $h_1 \rightarrow b\bar{b}$ is the dominant decay channel of h_1 since the Yukawa coupling of h_1 with bottom quark is usually much larger than its couplings with the other light quarks and leptons.
- (iii) An uncertainty of 10% in C_{h_2VV} measurement by the latest Higgs data at the LHC [3] implies that $|C_{h_1VV}|^2 \lesssim 0.2$. This size is large enough to produce the central value of the $b\bar{b}$ excess because $\text{Br}(h_1 \rightarrow b\bar{b})$ is insensitive to $C_{h_1b\bar{b}}$ unless it is suppressed too much [see Eq. (2.14)].
- (iv) A moderately large $C_{h_1\gamma\gamma}^{\tilde{\chi}^\pm}$ (compared with the top- and W-loop contribution) together with a suppressed $C_{h_1b\bar{b}}$ (relative to $C_{h_1\tilde{t}\tilde{t}}$) is favored to explain the diphoton excess.⁵ This can be understood by the fact

⁵Note that similar conditions to enhance the ratio $\text{Br}(h_1 \rightarrow \gamma\gamma)/\text{Br}_{\text{SM}}(h_1 \rightarrow \gamma\gamma)$ in supersymmetric theories have been obtained in [62,63].

$$\begin{aligned} \frac{\mu_{\text{CMS}}}{\mu_{\text{LEP}}} &= \frac{C_{h_1gg}^2}{C_{h_1VV}^2} \times \frac{C_{h_1\gamma\gamma}^2}{C_{h_1b\bar{b}}^2} \simeq \frac{C_{h_1\gamma\gamma}^2}{C_{h_1b\bar{b}}^2} \\ &\simeq \left(\frac{V_{12} + C_{h_1\gamma\gamma}^{\tilde{\chi}^\pm}}{V_{11} \tan\beta + V_{12}} \right)^2 \sim 5, \end{aligned} \quad (2.17)$$

where the number 5 is obtained from the central values of the excesses in Eq. (1.2). This formula reveals that if $C_{h_1\gamma\gamma}^{\tilde{\chi}^\pm} \simeq 0$, the condition $V_{11} \tan\beta \simeq -0.55V_{12}$ must be satisfied to predict the excesses. This will put strong constraint on the parameter space of the Type-I NMSSM, while a varying $C_{h_1\gamma\gamma}^{\tilde{\chi}^\pm}$ can relax the correlation.

III. EXPLANATIONS OF THE EXCESSES

In this section, we attempt to explain the excesses in the NMSSM with the Type-I seesaw mechanism. We utilize the package SARAH-4.11.0 [64–66] to build the model, the codes SPheno-4.0.3 [67] and FlavorKit [68] to generate particle spectrum and compute low energy flavor observables, respectively, the package HiggsBounds-5.3.2 [69] and HiggsSignals-2.2.3 [70] to implement the constraints from the direct search for extra Higgs bosons at LEP, Tevatron, and LHC. For some benchmark settings, we also use the package MicrOMEGAs4.3.4 [71–73] to compute DM observables by assuming the lightest sneutrino as the only DM candidate in the Universe. In calculating the radiative correction to the Higgs mass spectrum, the code SPheno-4.0.3 only includes full one- and two-loop effects using a diagrammatic approach with vanishing external momenta [67]. This leaves an uncertainty of about 2 GeV for the SM-like Higgs boson mass.

A. Strategy in scanning the parameter space

Previous discussions indicate that only the parameters in the Higgs sector determine the $b\bar{b}$ and $\gamma\gamma$ signals. We perform a sophisticated scan over these inputs and the soft trilinear coefficient A_t for top squark (since this parameter can affect significantly the Higgs mass spectrum by radiative corrections) in the following ranges⁶:

$$\begin{aligned} 0 < \lambda \leq 0.75, \quad 0 < \kappa \leq 0.75, \quad 1 \leq \tan\beta \leq 20, \\ 100 \text{ GeV} \leq \mu \leq 600 \text{ GeV}, \quad 300 \text{ GeV} \leq A_\lambda \leq 2 \text{ TeV}, \\ -1 \text{ TeV} \leq A_\kappa \leq 0 \text{ TeV}, \quad |A_t| \leq 5 \text{ TeV}, \end{aligned} \quad (3.1)$$

where all the parameters are defined at the scale $Q = 1 \text{ TeV}$. The other unimportant parameters are set as follows: $\lambda_\nu = 0.1$, $M_1 = M_2 = 2 \text{ TeV}$, and $M_3 = 5 \text{ TeV}$ for gaugino soft breaking masses, and all soft breaking

⁶Note that we are not intend to perform a complete fit of the model to the excesses in this work, so we only select by experienced part of its parameter space for study.

parameters in squark and slepton sectors except A_t are fixed at 2 TeV, which are consistent with the results of the LHC search for sparticles. In the scan, we adopt the MultiNest algorithm in [74] with the flat distribution for the inputs and $n\text{live} = 10\,000$, and construct the likelihood function

$$\mathcal{L} = \mathcal{L}_{\text{excess}} \times \mathcal{L}_{h_2, \text{mass}} \equiv \text{Exp} \left[-\frac{1}{2} \chi_{\text{H}}^2 \right] \quad (3.2)$$

to guide the scan, where $\chi_{\text{H}}^2 = \chi_{\text{excess}}^2 + \chi_{h_2, \text{mass}}^2$ with χ_{excess}^2 and $\chi_{h_2, \text{mass}}^2$ denoting the χ^2 function of the excesses and m_{h_2} , respectively, and their forms given by⁷

$$\chi_{\text{excess}}^2 = \left(\frac{m_{h_1} - 96.0}{0.2} \right)^2 + \left(\frac{\mu_{\text{LEP}} - 0.117}{0.057} \right)^2 + \left(\frac{\mu_{\text{CMS}} - 0.6}{0.2} \right)^2, \quad (3.3)$$

$$\chi_{h_2, \text{mass}}^2 = \left(\frac{m_{h_2} - 125.1}{2.0} \right)^2. \quad (3.4)$$

Note that the setting $n\text{live}$ in the MultiNest method denotes the number of active or live points used to determine the iso-likelihood contour in each iteration [74,75]. The larger it is, the more meticulous the scan becomes in surveying the parameter space.

In the scan, we also calculate the following χ^2 functions for each sample:

- (i) $\chi_{h_2, \text{couplings}}^2$ for seven couplings of the discovered Higgs boson in the κ framework, which were recently obtained by ATLAS Collaboration with 80 fb^{-1} data. We assume no exotic decay of h_2 , and use the coupling information for the scenario (a) in Table 11 of [3] and its corresponding correlation matrix in Figure 38 of the same experimental report to calculate the $\chi_{h_2, \text{couplings}}^2$. We do not include the theoretical uncertainty in calculating the couplings since they are much smaller than corresponding experimental uncertainty.
- (ii) χ_B^2 for the measurement of $\text{Br}(B \rightarrow X_s \gamma)$ and $\text{Br}(B_s \rightarrow \mu^+ \mu^-)$, which takes the form [76]

$$\chi_B^2 = \frac{(B_\gamma - 3.43)^2}{0.4^2} + \frac{(B_{\mu^+ \mu^-} - 3.11)^2}{1.2^2}$$

⁷We assume relatively small total (theoretical and experimental) uncertainties for m_{h_1} and m_{h_2} in the study, i.e., $\Delta m_{h_1} = 0.2 \text{ GeV}$ and $\Delta m_{h_2} = 2 \text{ GeV}$, to ensure that the samples obtained in the scan focus on the case $m_{h_1} \simeq 96 \text{ GeV}$ and $m_{h_2} \simeq 125 \text{ GeV}$. Moreover, we do not include the coupling information of the discovered Higgs boson in the \mathcal{L} because we want to get the best explanations to the excess instead of to perform a global fit of the model with all experimental data. This is vital in our calculation since so far the excesses are not very significant.

with B_γ and $B_{\mu^+ \mu^-}$ denoting the theoretical prediction of $\text{Br}(B \rightarrow X_s \gamma)$ and $\text{Br}(B_s \rightarrow \mu^+ \mu^-)$ in unit of 10^{-4} and 10^{-9} , respectively.

- (iii) χ_{EW}^2 for precision electroweak measurements ϵ_i ($i = 1, 2, 3$) [77–79] or equivalently S , T , and U parameters [80,81]. We use the formulas for the self-energies of the gauge bosons γ , W^\pm , and Z in [82] to calculate these observables, and the fit results in [83] to get the χ_{EW}^2 .

In getting the explanations of the excesses, we refine the samples obtained in the scan by the following conditions: $m_{A_1} > m_{h_2}/2$ so that the discovered Higgs boson has no exotic decay, $\lambda^2 + \kappa^2 \leq 0.5$ so that the theory keeps perturbative up to 10^{16} GeV scale [84], $\chi_{h_2, \text{coupling}}^2 \leq 14.1$ which is 95% confidence level exclusion limit of the Higgs couplings for 7 degrees of freedom, and $\chi_{\text{tot}}^2 \leq 18.6$ with χ_{tot}^2 defined by⁸

$$\chi_{\text{tot}}^2 = \chi_{\text{excess}}^2 + \chi_{h_2, \text{mass}}^2 + \chi_{h_2, \text{couplings}}^2 + \chi_B^2 + \chi_{\text{EW}}^2. \quad (3.5)$$

We also require the samples to survive the constraints from the HiggsBounds.

At this stage, we remind that, if one does not consider the constraints from DM physics and the relevant sparticle searches at the LHC, the Higgs physics of the NMSSM is same as that of the extended model. So one may also use the package NMSMTools [85,86] to perform the scan. We compare the NMSMTools with our toolkit, and find that their explanations of the excesses shown in the following figures are similar, although the NMSMTools is somewhat faster than our toolkit in calculation.

B. Numerical results

Based on the samples obtained in the scan, we plot the PLs of the \mathcal{L} in Eq. (3.2) on different planes,⁹ where the color bar in Figs. 1–3 represents the PL value relative to the best point marked by star symbol, and the white and pink

⁸ χ_{tot}^2 denotes a measure of the agreement between the theory and the total experimental data considered in this work. In this hypothesis, the goodness-of-fit measure χ_{tot}^2 obeys a χ^2 distribution with $N_{\text{obs}} - N_{\text{para}} + 1$ degree of freedom (d.o.f.). In our study, the d.o.f. is $16 - 7 + 1 = 10$, and $\chi_{\text{tot}}^2 = 18.6$ corresponds to the upper limit of χ_{tot}^2 at 2σ confidence level.

⁹The frequentist PL is defined as the largest likelihood value in a certain parameter space [87]. Given a likelihood function \mathcal{L} defined in N -dimensional space $\Theta = (\Theta_1, \Theta_2, \dots, \Theta_N)$, its two-dimensional PL can be obtained by the procedure

$$\mathcal{L}(\Theta_i, \Theta_j) = \max_{\Theta_1, \dots, \Theta_{i-1}, \Theta_{i+1}, \dots, \Theta_{j-1}, \Theta_{j+1}, \dots, \Theta_N} \mathcal{L}(\Theta).$$

Obviously, the PL reflects the preference of a theory on the parameter space, and for a given point on $\Theta_i - \Theta_j$ plane, the value of $\mathcal{L}(\Theta_i, \Theta_j)$ represents the capability of the point in the theory to account for experimental data by varying the other parameters.

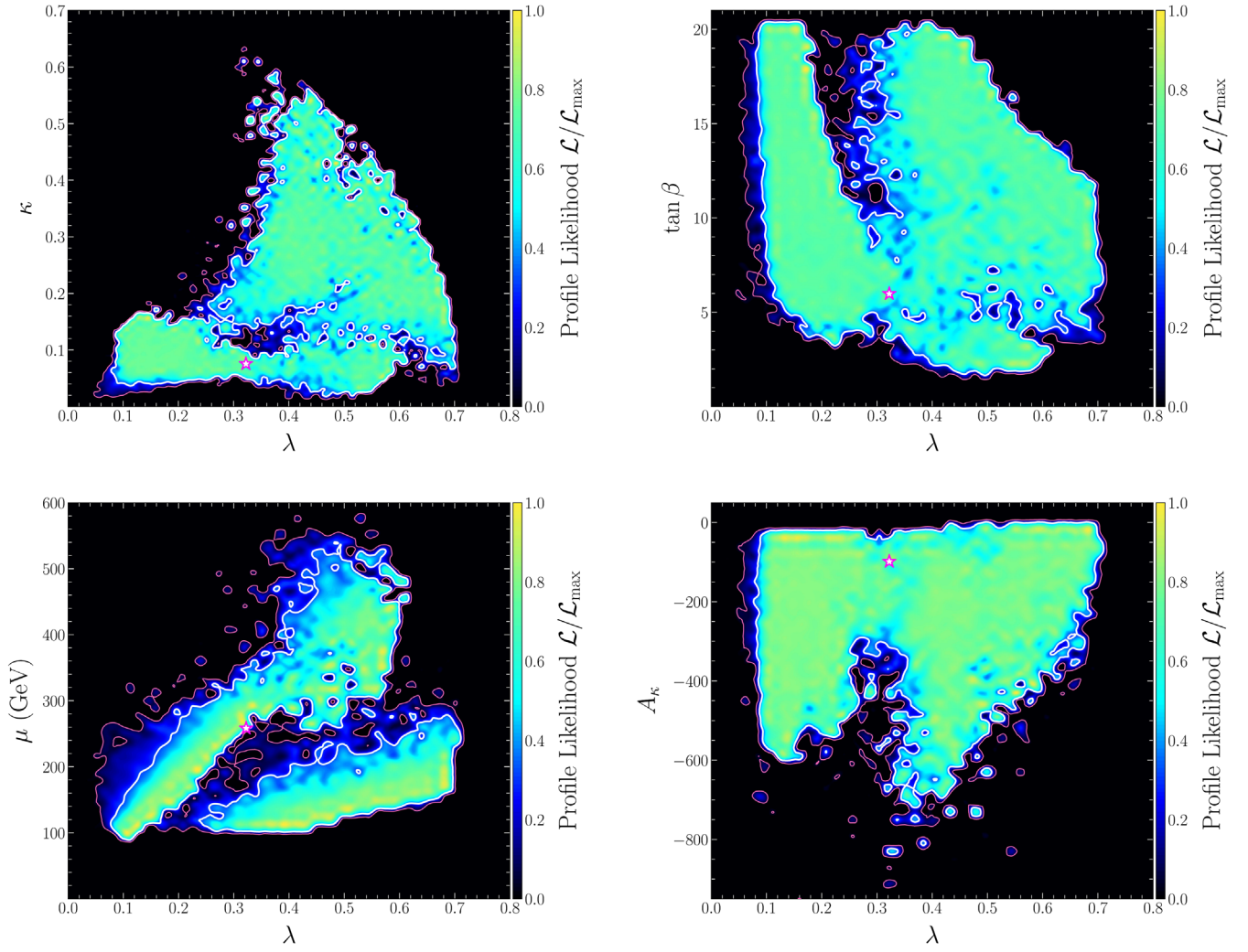


FIG. 1. Two dimensional profile likelihood of \mathcal{L} in Eq. (3.2), which are projected on $\kappa - \lambda$, $\tan\beta - \lambda$, $\mu - \lambda$, and $A_\kappa - \lambda$ planes, respectively. Since $\chi^2_{H,\min} \simeq 0$ for the best point (marked by star symbol in the figure), the 1σ boundary (white solid line) and the 2σ boundary (red line) correspond to $\chi^2_H \simeq 2.3$ and $\chi^2_H \simeq 6.18$, respectively. This figure reflects the preference of the excesses on the parameter space of the extended NMSSM. Note that all samples in this figure satisfy the conditions above Eq. (3.5), especially $\chi^2_{h_2,\text{coupling}} \leq 14.1$, so they are consistent with the data for the discovered Higgs boson at 2σ level.

solid lines are boundaries for 1σ and 2σ confidence intervals (CIs), respectively. Figure 1 indicates that there is broad parameter space to explain the excesses, and the large deviation between the 1σ and 2σ boundaries on $\mu - \lambda$ plane reflects that the explanation is sensitive to the parameters λ and μ . Figure 2 shows that the magnitude of the normalized couplings of h_1 may reach 0.5 except $|C_{h_1 b\bar{b}}|$ which is relatively suppressed. The best point for the excesses predicts $C_{h_1 VV} = -0.36$, $C_{h_1 gg} = -0.38$, $C_{h_1 \gamma\gamma} = -0.41$, $C_{h_1 t\bar{t}} = -0.37$, and $C_{h_1 b\bar{b}} = -0.18$, and consequently $\text{Br}(h_1 \rightarrow b\bar{b}) = 65\%$ and $\text{Br}(h_1 \rightarrow \gamma\gamma) = 0.6\%$. The pattern $\text{Br}(h_1 \rightarrow b\bar{b})/\text{Br}_{\text{SM}}(H \rightarrow b\bar{b}) < 1$ and $\text{Br}(h_1 \rightarrow \gamma\gamma)/\text{Br}_{\text{SM}}(H \rightarrow \gamma\gamma) \simeq 3.7$ agrees well with the expectation in Sec. II. Moreover, a closer analysis of the samples reveals that the explanations are distributed in three isolated parameter regions

- (i) Region I: $0.06 \lesssim \lambda \lesssim 0.37$, $0.03 \lesssim \kappa \lesssim 0.17$, $4 \lesssim \tan\beta \lesssim 20$, $100 \text{ GeV} \lesssim \mu \lesssim 350 \text{ GeV}$, and $\mu/\lambda \sim 800 \text{ GeV}$.
- (ii) Region II: $0.22 \lesssim \lambda \lesssim 0.7$, $0.06 \lesssim \kappa \lesssim 0.6$, $4 \lesssim \tan\beta \lesssim 20$, $100 \text{ GeV} \lesssim \mu \lesssim 300 \text{ GeV}$, and $\mu/\lambda \sim 250 \text{ GeV}$.
- (iii) Region III: $0.37 \lesssim \lambda \lesssim 0.6$, $0.02 \lesssim \kappa \lesssim 0.14$, $2 \lesssim \tan\beta \lesssim 5$, and $250 \text{ GeV} \lesssim \mu \lesssim 560 \text{ GeV}$.

They are characterized by the following:

- (i) The posterior probabilities of the three regions are 0.80, 0.16, and 0.04, respectively.¹⁰ This reflects the fact that the Region I is more likely to explain the excesses.

¹⁰The concept of the posterior probability comes from Bayesian theorem, which was briefly introduced in [87].

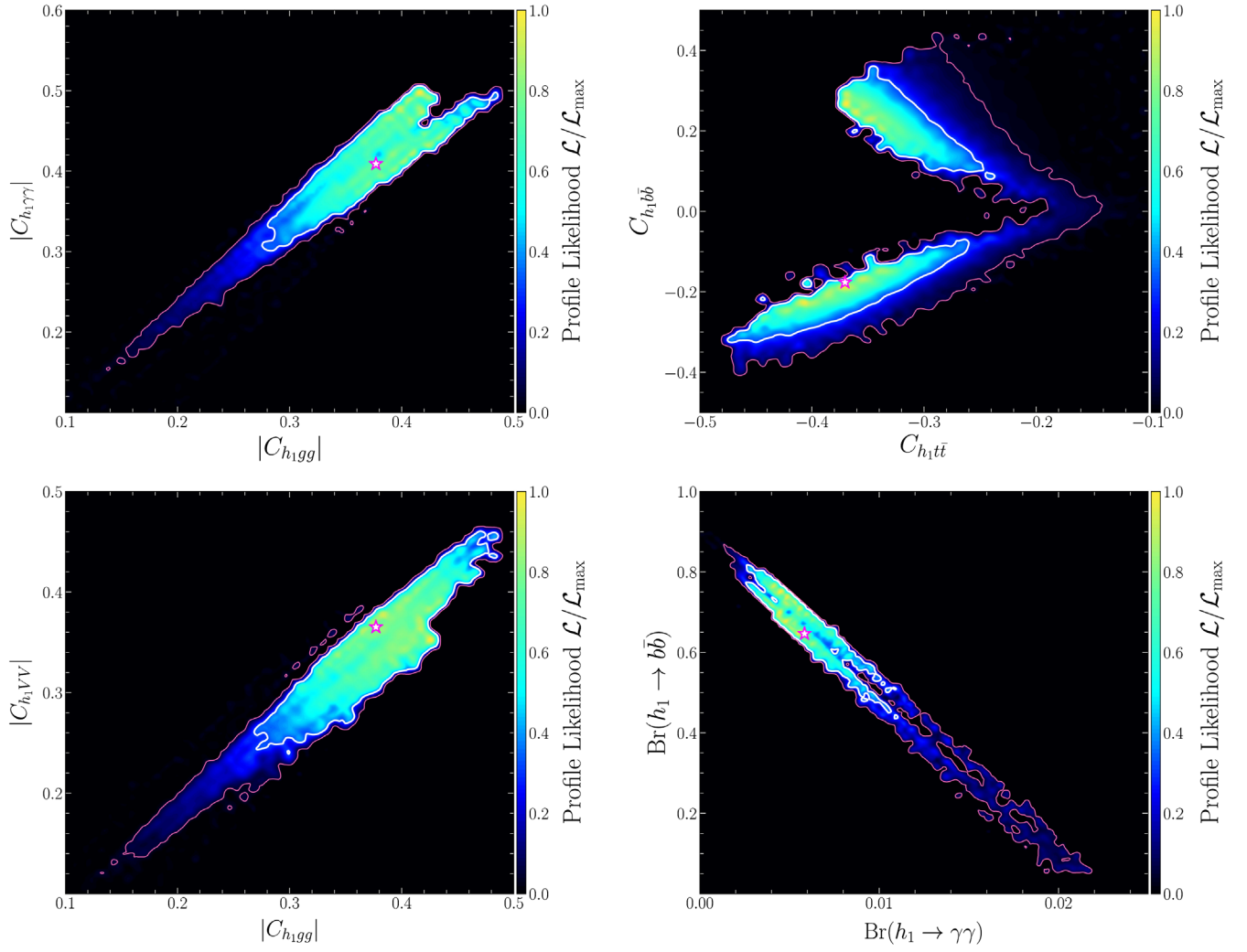


FIG. 2. Similar to Fig. 1, but projected on $|C_{h_1\gamma\gamma}| - |C_{h_1gg}|$, $C_{h_1b\bar{b}} - C_{h_1t\bar{t}}$, $|C_{h_1VV}| - |C_{h_1gg}|$, and $\text{Br}(h_1 \rightarrow \gamma\gamma) - \text{Br}(h_1 \rightarrow b\bar{b})$ planes, respectively.

- (ii) In both *Regions I* and *Region II*, the lightest neutralino $\tilde{\chi}_1^0$ may be either Higgsino dominated or Singlino dominated (corresponding to $2\kappa/\lambda > 1$ and $2\kappa/\lambda < 1$, respectively [25]), while in *Region III*, $\tilde{\chi}_1^0$ is only Singlino dominated.
- (iii) All the regions are able to predict the central value of the excesses. In *Regions I* and *III*, the most favored parameter points predict $\chi_{h_2, \text{couplings}}^2 \sim 7$, while those in *Region II* usually predict $\chi_{h_2, \text{couplings}}^2 > 10$. This fact reflects that there is minor tension between the excesses and the data of the discovered Higgs for *Region II*.
- (iv) *Regions I* and *II* correspond to the lower and upper branches of the first panel in Fig. 2, respectively. For both the branches, V_{12} in Eq. (2.15) is always negative, and $C_{h_1b\bar{b}}$ may be either negative (the lower branch) or positive (the upper branch) due to the moderate/strong cancellation between $V_{11} \tan\beta$ and V_{12} in the expression of $C_{h_1b\bar{b}}$. Similar conclusion applies to the other panels in Fig. 2.

- (v) For all the regions, $m_{H^\pm} \gtrsim 550$ GeV which is consistent with the results in [22] for a general NMSSM, and A_1 may be lighter than 100 GeV.

We also study the couplings of the SM-like Higgs boson in Fig. 3. This figure shows that the normalized couplings C_{h_2VV} , $C_{h_2\gamma\gamma}$, C_{h_2gg} , and $C_{h_2t\bar{t}}$ are centered around 0.92, and $C_{h_2b\bar{b}}$ may reach 1.2. $\text{Br}(h_2 \rightarrow b\bar{b})$ varies from 0.55 to 0.75 in comparison with its SM prediction 0.575 ± 0.018 , and $\text{Br}(h_2 \rightarrow \gamma\gamma)$ changes from 1.3×10^{-3} to 2.2×10^{-3} with its SM prediction $(2.28 \pm 0.11) \times 10^{-3}$ [60]. As pointed out in [17], the sizable deviation of the couplings from its SM predictions and the presence of h_1 can be explored by future high luminosity LHC or e^+e^- colliders.

IV. CONSTRAINTS FROM DM PHYSICS AND SPARTICLE SEARCH

So far, we do not consider the constraints from DM physics and the LHC search for sparticles on the regions.

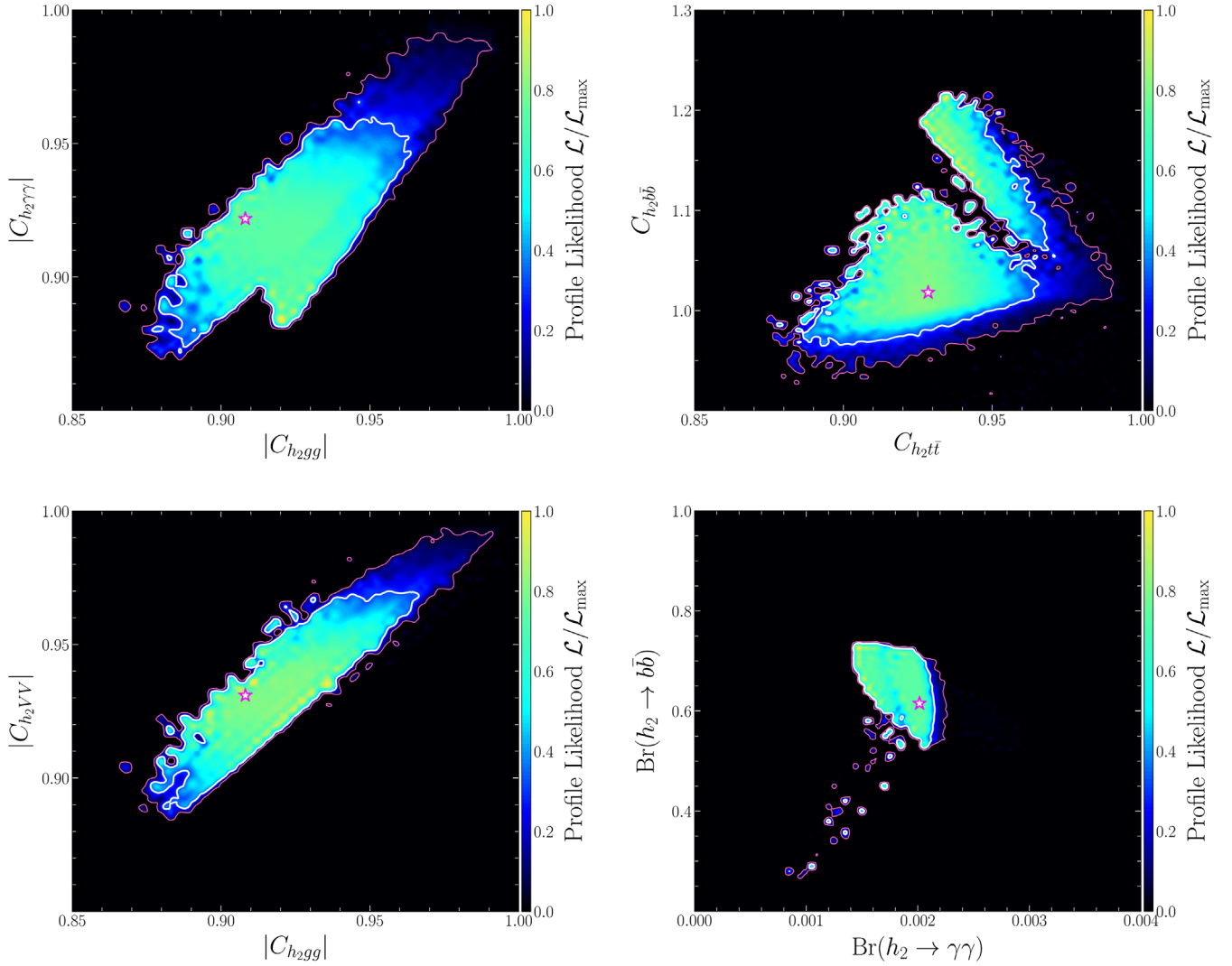


FIG. 3. Similar to Fig. 1, but projected on $C_{h_2\gamma\gamma} - C_{h_2gg}$, $C_{h_2b\bar{b}} - C_{h_2t\bar{t}}$, $C_{h_2VV} - C_{h_2gg}$, and $\text{Br}(h_2 \rightarrow \gamma\gamma) - \text{Br}(h_2 \rightarrow b\bar{b})$ planes, respectively.

For each sample obtained from the scan in last section, these constraints can be implemented by the following procedures [44]:

- (i) Vary the parameters λ_ν , A_{λ_ν} , and $m_{\tilde{\nu}}$ in the sneutrino sector,¹¹ and select the sample for which the right-handed sneutrino with τ flavor is lighter than the other sparticles. To be consistent with the Higgs data fit in the previous section, the decay channels $h_1 \rightarrow \nu_h \bar{\nu}_h$, $h_2 \rightarrow \nu_h \bar{\nu}_h$, $h_1 \rightarrow \tilde{\nu}_1 \tilde{\nu}_1$, and $h_2 \rightarrow \tilde{\nu}_1 \tilde{\nu}_1$ (ν_h denotes a heavy neutrino with the field ν as its dominant component) are kinematically forbidden.

¹¹Since the soft breaking parameter A_ν is always associated with the Yukawa coupling Y_ν [see the term $Y_\nu A_\nu \tilde{\nu}_R^* \tilde{H}_u$ in Eq. (2.1)] and $Y_\nu \sim 10^{-6}$, the results in this section are insensitive to the value of A_ν when $|A_\nu|$ is less than several TeV. So, we fix $A_\nu = 2$ TeV throughout this work.

Since $m_{\nu_h} = 2\lambda_\nu \mu / \lambda$, these requirements are equivalent to

$$\lambda_\nu \geq \lambda \times \frac{m_{h_2}}{4\mu}, \quad m_{\tilde{\nu}_1} \geq \frac{m_{h_2}}{2}.$$

- (ii) Take the sneutrino as the only DM candidate, calculate the quantities such as DM relic density, its scattering rate with nucleon and the photon spectrum of its annihilation in dwarf galaxies, and compare them with relevant measurements of the Planck experiment, the XENON-1T experiment, and the Fermion-LAT experiment, respectively.
- (iii) Study the signals of electroweakino production processes at the LHC, and check by simulations whether the signals coincide with the LHC results.

Since the involved calculations are rather complex and meanwhile more than 0.1 million samples were accumulated

TABLE II. Benchmark point of Region I with dimensional parameters in unit of GeV. Note that the normalized coupling $C_{h_2 ii^*}$ ($i = Z, W, b, t, \tau, \gamma, g$) is equivalent to κ_i defined in Table 36 of [60], $\mu_{ggF}^{\gamma\gamma}$ denotes the normalized signal strength of h_2 for diphoton decay channel in the gluon fusion production mode, and μ_{ggF}^{ZZ} and $\mu_{VH}^{b\bar{b}}$ have similar definition to $\mu_{ggF}^{\gamma\gamma}$. Since $C_{h_2 ZZ} \equiv C_{h_2 WW}$ in the theory, $\mu_{ggF}^{WW} = \mu_{ggF}^{ZZ}$ [60]. This table shows that, in order to explain the excesses, the normalized couplings of h_2 are around 0.9 and the signal strengths range from 0.7 to 0.9. This fact reflects a moderate tension between the excesses and the data of the discovered Higgs boson.

λ	0.164	$\chi_{h_2, \text{coupling}}^2$	7.97	m_{h_1}	95.9	$\text{Br}(h_1 \rightarrow \gamma\gamma)$	4.88×10^{-3}
κ	0.112	$C_{h_2 ZZ}$	0.918	m_{h_2}	124.6	$\text{Br}(h_1 \rightarrow b\bar{b})$	0.626
$\tan\beta$	19.24	$C_{h_2 WW}$	0.918	m_{h_3}	2332.9	$C_{h_1 gg}$	0.4152
μ	147.7	$C_{h_2 b\bar{b}}$	0.999	m_{A_1}	301.8	$C_{h_1 VV}$	0.398
A_λ	1785.1	$C_{h_2 i\bar{i}}$	0.917	m_{A_2}	2332.8	V_{11}	0.0115
A_κ	-304.6	$C_{h_2 \tau\bar{\tau}}$	0.999	m_{H^\pm}	2348.9	V_{12}	0.3982
A_t	1354.7	$C_{h_2 \gamma\gamma}$	0.907	$m_{\chi_1^0}$	145.1	V_{13}	-0.9172
$\mu_{ggF}^{\gamma\gamma}$	0.735	$C_{h_2 gg}$	0.919	$m_{\chi_2^0}$	155.8	μ_{CMS}	0.588
μ_{ggF}^{ZZ}	0.753	$\mu_{VH}^{b\bar{b}}$	0.893	$m_{\chi_1^\pm}$	152.9	μ_{LEP}	0.119

in the scan, it is very time consuming to check all the samples with the constraints. Instead, we only consider one benchmark setting for each of the three regions and illustrate its underlying physics.

Let us first consider the benchmark setting of Region I, whose information is presented in Table II. We perform a further scan over the following region:

$$0 < m_\nu < 150 \text{ GeV}, \quad 0 < \lambda_\nu < 0.5, \quad |A_{\lambda_\nu}| < 1 \text{ TeV}, \quad (4.1)$$

with the MultiNest algorithm by requiring $m_{\nu_R} > m_{h_1}/2$ and assuming the sneutrino DM to be CP even. The likelihood function we adopt is composed by

$$\mathcal{L}_{\text{DM}} = \mathcal{L}_{\Omega_{\tilde{\nu}_1}} \times \mathcal{L}_{\text{DD}} \times \mathcal{L}_{\text{ID}}, \quad (4.2)$$

where $\mathcal{L}_{\Omega_{\tilde{\nu}_1}}$, \mathcal{L}_{DD} , and \mathcal{L}_{ID} account for the relic density, the XENON-1T experiment and the Fermi-LAT observation of dwarf galaxy, respectively, and their explicit forms are presented in [44].

In the left panel of Fig. 4, we present the profile likelihood of the \mathcal{L}_{DM} for the setting in Table II on $\lambda_\nu - m_{\tilde{\nu}_1}$ plane with $m_{\tilde{\nu}_1}$ denoting the DM mass. This panel shows that the mass of $\tilde{\nu}_1$ is roughly degenerate with the Higgsino mass μ , which implies that the DM gets the right relic density through coannihilating with the Higgsinos [44]. Given that $\tilde{\chi}_1^0$ and $\tilde{\chi}_2^0$ in this setting decay by $\tilde{\chi}_{1,2}^0 \rightarrow \nu_\tau \tilde{\nu}_1$ and thus they correspond to missing momentum at the LHC, the most promising channel to probe the Higgsinos is through the process $pp \rightarrow \tilde{\chi}_1^\pm \tilde{\chi}_1^\mp \rightarrow (\tau^\pm \tilde{\nu}_1)(\tau^\mp \tilde{\nu}_1)$ [44]. Obviously, the LHC has no capability to exclude the moderately light Higgsinos since the τ leptons are soft due to the compressed mass spectrum of $\tilde{\chi}_1^\pm$ and $\tilde{\nu}_1$ [44]. The panel also shows that λ_ν is upper bounded by about 0.1, which means that the DM cannot annihilate by the channel $\tilde{\nu}_1 \tilde{\nu}_1 \rightarrow h_1 h_1$ to get its right relic density (see the formula of

the relic density in various simple DM theories [88,89]). This is mainly due to the constraint from the DM DD experiments, which may be understood as follows: in the seesaw extension of the NMSSM, the $\tilde{\nu}_1$ -nucleon scattering proceeds mainly by the t -channel exchange of CP -even Higgs bosons, and any large $\tilde{\nu}_1 \tilde{\nu}_1 h_1$ or $\tilde{\nu}_1 \tilde{\nu}_1 h_2$ coupling is dangerous to spoil the XENON-1T bound. For a CP -even $\tilde{\nu}_1$, the involved coupling strength is given by [44]

$$C_{\tilde{\nu}_1 \tilde{\nu}_1 h_i} = \frac{\lambda \lambda_\nu M_W}{g} (\sin \beta Z_{i1} + \cos \beta Z_{i2}) - \left[\frac{\sqrt{2}}{\lambda} (2\lambda_\nu^2 + \kappa \lambda_\nu) \mu - \frac{\lambda_\nu A_{\lambda_\nu}}{\sqrt{2}} \right] Z_{i3}, \quad (4.3)$$

where Z_{ij} ($i, j = 1, 2, 3$) denote the elements of the matrix to diagonalize the CP -even Higgs mass matrix in the basis ($\text{Re}[H_d^0]$, $\text{Re}[H_u^0]$, $\text{Re}[S]$) with their values given in Table II. With regard to the specific setting, $C_{\tilde{\nu}_1 \tilde{\nu}_1 h_1}/\lambda_\nu$ gets a far dominant contribution from the second bracket in Eq. (4.3), and it is quite large (exceeding 200 GeV) since $\mu/\lambda \sim 900$ GeV and A_{λ_ν} is negative.¹² The situation of $C_{\tilde{\nu}_1 \tilde{\nu}_1 h_2}/\lambda_\nu$ is quite similar since $|Z_{23}| = 0.39$ is not a small number. Then with the mass insertion method, one can estimate the cross section of the scattering by [46]

$$\begin{aligned} \sigma_{\tilde{\nu}_1-p}^{SI} &\propto \left\{ \sum_{i=1}^3 (a_{u,i} + a_{d,i}) \right\}^2 \\ &\propto \frac{g^2}{16m_W^2} \times \left\{ \frac{1}{m_{\tilde{\nu}_1}} \left[\frac{\sqrt{2}}{\lambda} (2\lambda_\nu^2 + \kappa \lambda_\nu) \mu - \frac{\lambda_\nu A_{\lambda_\nu}}{\sqrt{2}} \right] \frac{m_{h_2}^2 - m_{h_1}^2}{m_{h_1}^2 m_{h_2}^2} \right\}^2 \\ &\quad \times Z_{13}^2 (1 - Z_{13})^2. \end{aligned}$$

¹²As shown by the sneutrino mass matrix in [44], a negative A_{λ_ν} is needed to ensure that a CP -even sneutrino state is lighter than its CP -odd partner.

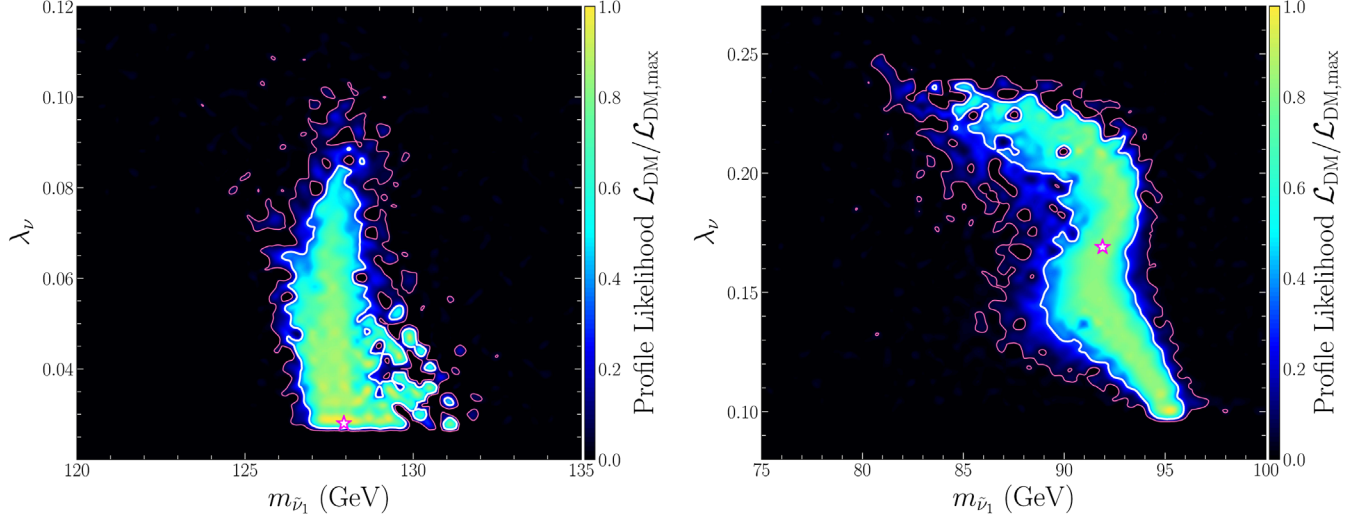


FIG. 4. The map for the profile likelihood of \mathcal{L}_{DM} in Eq. (4.2), which is plotted on $\lambda_\nu - m_{\tilde{\nu}_1}$ plane. Given that $\chi_{\text{DM,min}}^2 \simeq 0$ for the best point which is marked by star symbol, the 1σ boundary (white solid line) and the 2σ boundary (red line) correspond to $\chi_{\text{DM}}^2 \simeq 2.3$ and $\chi_{\text{DM}}^2 \simeq 6.18$, respectively. The left panel is for the setting of Region I, and the right panel is for the setting of Region II.

We checked that this formula is a good approximation of the exact cross section in [44] for the parameter setting. So, in order to survive the XENON-1T constraint, λ_ν must be upper bounded by about 0.1 and correspondingly the coannihilation channel is dominant. This usually predicts the SI cross section varying from 10^{-48} to 10^{-47} cm², but in some rare cases it may be below 10^{-50} cm². We checked that this conclusion also applies to the case with a CP -odd sneutrino DM, where, although A_{λ_ν} may be either positive or negative to get a CP -odd sneutrino DM [44], its magnitude is limited so that it cannot cancel the contribution of the $\sqrt{2}\mu(2\lambda_\nu^2 + \kappa\lambda_\nu)/\lambda$ term in an efficient way.

Next we turn to the setting of the Region II in Table III, which is featured by $\mu/\lambda \simeq 326$ GeV and $\lambda_\nu \gtrsim 0.08$. Similar to what we did for Region I, we plot the profile likelihood on $\lambda_\nu - m_{\tilde{\nu}_1}$ plane and show the boundaries of 1σ CI (white solid line) and 2σ CI (red line) on the right panel of Fig. 4. We find that the samples in the 2σ CI annihilated mainly by the channel $\tilde{\nu}_1\tilde{\nu}_1 \rightarrow h_1h_1$ in early universe. This annihilation requires $\lambda_\nu \sim 0.15$ to get the right relic density [88,89], and due to the temperature effect, $\tilde{\nu}_1$ may be lighter than h_1

in proceeding the annihilation [48]. We also find that the samples predict the scattering cross section ranging from 10^{-51} to 3×10^{-47} cm², and the constraints from current DM DD experiments are relatively weak. Same as the previous setting, the Higgsinos may be probed by the process $pp \rightarrow \tilde{\chi}_1^\pm \tilde{\chi}_1^\mp \rightarrow (\tau^\pm \tilde{\nu}_1)(\tau^\mp \tilde{\nu}_1)$. From the simulation results in [44], the regions of $\mu \lesssim 170$ GeV and $\mu \gtrsim 280$ GeV can survive the LHC constraints for the DM mass given in the panel.

Finally, we consider the benchmark setting of Region III in Table IV. Different from the other settings, now $\tilde{\chi}_1^0$ and $\tilde{\chi}_{2,3}^0$ are Singlino and Higgsino dominated, respectively, with their field compositions given by

$$\begin{aligned}
 \tilde{\chi}_1^0 &= 0.006\tilde{B}^0 - 0.010\tilde{W}^0 + 0.058\tilde{H}_d^0 - 0.233\tilde{H}_u^0 + 0.971\tilde{S}^0, \\
 \tilde{\chi}_2^0 &= -0.020\tilde{B}^0 + 0.038\tilde{W}^0 - 0.707\tilde{H}_d^0 + 0.676\tilde{H}_u^0 + 0.205\tilde{S}^0, \\
 \tilde{\chi}_3^0 &= -0.010\tilde{B}^0 + 0.019\tilde{W}^0 + 0.705\tilde{H}_d^0 + 0.698\tilde{H}_u^0 + 0.125\tilde{S}^0.
 \end{aligned}
 \tag{4.4}$$

TABLE III. Same as Table II, but for the benchmark setting of Region II.

λ	0.355	$\chi_{h_2, \text{coupling}}^2$	8.73	m_{h_1}	96.1	$\text{Br}(h_1 \rightarrow \gamma\gamma)$	5.42×10^{-3}
κ	0.433	C_{h_2ZZ}	0.947	m_{h_2}	125.1	$\text{Br}(h_1 \rightarrow b\bar{b})$	0.672
$\tan\beta$	15.66	C_{h_2WW}	0.947	m_{h_3}	1623.2	C_{h_1gg}	0.361
μ	115.9	$C_{h_2b\bar{b}}$	1.135	m_{A_1}	453.3	C_{h_1VV}	0.321
A_λ	1319.1	$C_{h_2\tilde{t}\tilde{t}}$	0.946	m_{A_2}	1622.4	V_{11}	0.0134
A_κ	-502.1	$C_{h_2\tilde{\tau}\tilde{\tau}}$	1.135	m_{H^\pm}	1617.5	V_{12}	-0.3229
A_t	1901.5	$C_{h_2\gamma\gamma}$	0.918	$m_{\tilde{\chi}_1^0}$	109.0	V_{13}	-0.9463
$\mu_{ggF}^{\gamma\gamma}$	0.653	C_{h_2gg}	0.943	$m_{\tilde{\chi}_2^0}$	126.4	μ_{CMS}	0.495
μ_{ggF}^{ZZ}	0.694	$\mu_{VH}^{b\bar{b}}$	0.999	$m_{\tilde{\chi}_1^\pm}$	119.7	μ_{LEP}	0.091

TABLE IV. Same as Table II, but for the benchmark setting of Region III.

λ	0.434	$\chi_{h_2, \text{coupling}}^2$	7.80	m_{h_1}	96.1	$\text{Br}(h_1 \rightarrow \gamma\gamma)$	5.74×10^{-3}
κ	0.091	$C_{h_2 ZZ}$	0.921	m_{h_2}	125.3	$\text{Br}(h_1 \rightarrow b\bar{b})$	0.579
$\tan\beta$	5.06	$C_{h_2 WW}$	0.921	m_{h_3}	1595.2	$C_{h_1 gg}$	0.419
μ	317.7	$C_{h_2 b\bar{b}}$	1.010	m_{A_1}	189.2	$C_{h_1 VV}$	0.389
A_λ	1467.1	$C_{h_2 i\bar{i}}$	0.918	m_{A_2}	1593.0	V_{11}	0.0379
A_κ	-175.3	$C_{h_2 \tau\bar{\tau}}$	1.010	m_{H^\pm}	1586.7	V_{12}	0.3891
A_t	1967.1	$C_{h_2 \gamma\gamma}$	0.909	$m_{\tilde{\chi}_1^0}$	132.7	V_{13}	-0.9204
$\mu_{ggF}^{\gamma\gamma}$	0.724	$C_{h_2 gg}$	0.917	$m_{\tilde{\chi}_2^0}$	330.3	μ_{CMS}	0.703
μ_{ggF}^{ZZ}	0.743	$\mu_{VH}^{b\bar{b}}$	0.893	$m_{\tilde{\chi}_1^\pm}$	324.0	μ_{LEP}	0.114

TABLE V. Summary of the DM physics and the LHC signals for Regions I–III discussed in the text.

Region	DM annihilation	DM DD constraint	LHC signal
Region I	$\frac{2\kappa}{\lambda} > 1$	$\tilde{\nu}_1 \tilde{H}$ coannihilation	Weak $\text{soft } 2\tau + E_T^{\text{miss}}$
	$\frac{2\kappa}{\lambda} < 1$	$\tilde{\nu}_1 \tilde{\nu}_1 \rightarrow h_1 h_1$	Strong $W^{(*)} Z^{(*)} + E_T^{\text{miss}}$
Region II	$\frac{2\kappa}{\lambda} > 1$	$\tilde{\nu}_1 \tilde{\nu}_1 \rightarrow h_1 h_1$	Weak $2\tau + E_T^{\text{miss}}$
	$\frac{2\kappa}{\lambda} < 1$	$\tilde{\nu}_1 \tilde{\nu}_1 \rightarrow h_1 h_1$	Weak $W^{(*)} Z^{(*)} + E_T^{\text{miss}}$
Region III	$\frac{2\kappa}{\lambda} < 1$	$\tilde{\nu}_1 \tilde{\nu}_1 \rightarrow h_1 h_1$	Moderately strong $W^{(*)} Z^{(*)} + E_T^{\text{miss}}$

In this case, $\tilde{\nu}_1$ is unlikely to coannihilate with $\tilde{\chi}_1^0$ to get the correct density because the couplings of $\tilde{\chi}_1^0$ with SM particles are rather weak, instead it annihilated mainly by the channels $\tilde{\nu}_1 \tilde{\nu}_1 \rightarrow h_i h_j$ with $i, j = 1, 2$ to get the density, which require $m_{\tilde{\nu}_1} \gtrsim 96$ GeV and $\lambda_\nu > 0.1$. Since λ_ν and $\mu/\lambda = 732$ GeV are large in comparison with the other settings, $\sigma_{\tilde{\nu}_1 p}^{\text{SI}} \gtrsim 1 \times 10^{-47}$ cm² for most cases, and consequently this benchmark setting is limited by the XENON-1T bound. The signals of these electroweakinos at the LHC are as follows. Due to the mass spectrum and field composition, $\tilde{\chi}_1^0$ decays by $\tilde{\chi}_1^0 \rightarrow \tilde{\nu}_1 \nu_\tau$ and thus corresponds to missing momentum, $\tilde{\chi}_{2,3}$ decay by the channels $\tilde{\chi}_{2,3}^0 \rightarrow Z\tilde{\chi}_1^0, h_1\tilde{\chi}_1^0, h_2\tilde{\chi}_1^0, A_1\tilde{\chi}_1^0$ with $\text{Br}(\tilde{\chi}_2^0 \rightarrow \tilde{\chi}_1^0 h_2) = 40\%$, $\text{Br}(\tilde{\chi}_2^0 \rightarrow \tilde{\chi}_1^0 Z) = 31.5\%$, $\text{Br}(\tilde{\chi}_3^0 \rightarrow \tilde{\chi}_1^0 h_2) = 12.5\%$, and $\text{Br}(\tilde{\chi}_3^0 \rightarrow \tilde{\chi}_1^0 Z) = 75.9\%$, and the Higgsino-dominated $\tilde{\chi}_1^\pm$ decays into $\tilde{\chi}_1^0 W^\pm$. The cross sections for the electroweakino pair productions are

$$\begin{aligned}
\sigma(pp \rightarrow \tilde{\chi}_1^0 \tilde{\chi}_1^0) &\simeq 8 \text{ fb}, & \sigma(pp \rightarrow \tilde{\chi}_1^0 \tilde{\chi}_2^0) &\simeq 3 \text{ fb}, \\
\sigma(pp \rightarrow \tilde{\chi}_1^0 \tilde{\chi}_3^0) &\simeq 10 \text{ fb}, & \sigma(pp \rightarrow \tilde{\chi}_1^\pm \tilde{\chi}_1^\pm) &\simeq 47 \text{ fb}, \\
\sigma(pp \rightarrow \tilde{\chi}_2^0 \tilde{\chi}_3^0) &\simeq 37 \text{ fb}, & \sigma(pp \rightarrow \tilde{\chi}_1^\pm \tilde{\chi}_1^\mp) &\simeq 38 \text{ fb}, \\
\sigma(pp \rightarrow \tilde{\chi}_2^0 \tilde{\chi}_1^\pm) &\simeq \sigma(pp \rightarrow \tilde{\chi}_3^0 \tilde{\chi}_1^\pm) &&\simeq 62.5 \text{ fb},
\end{aligned} \tag{4.5}$$

where we have set the collision energy of the LHC at 13 TeV and used the package MadGraph/MadEvent [90,91] in the calculation. These results indicate that the largest signal of the $\tilde{\chi}_1^0$ production is $pp \rightarrow \tilde{\chi}_1^0 \tilde{\chi}_1^\pm \rightarrow W^\pm + E_T^{\text{miss}}$

with its cross section about 50 fb. This rate, however, is much smaller than current upper bound on Mono-W signal search, which was more than 750 fb for $m_{\tilde{\chi}_1^0} = 132.7$ GeV by ATLAS analysis with an integrated 36.1 fb⁻¹ data [92]. The results also indicate that the best way to explore the setting may be through the process $pp \rightarrow \tilde{\chi}_{2,3} \tilde{\chi}_1^\pm \rightarrow ZW2\tilde{\chi}_1^0$ by trilepton plus E_T^{miss} signal. In fact, we calculate the R value of the signal by the analysis of CMS Collaboration with 35.9 fb⁻¹ data [93],¹³ like what we did in [35]. We find $R = 0.68$ which implies that the setting survives the LHC experiment.¹⁴ We also consider several other points in the region and find that the suppression of $\text{Br}(\tilde{\chi}_{2,3}^0 \rightarrow Z\tilde{\chi}_1^0)$ is vital to survive the collider constraint. Since these points predict $R > 0.5$, they may be detected by future LHC experiment.

Before we end this section, we have the following comments:

- (i) All the three benchmark settings can explain well the excesses and meanwhile keep consistent with the constraints from the DM physics and the LHC search for the electroweakinos by choosing appropriate λ_ν ,

¹³Note that the CMS analysis of the multilepton signal with 35.9 fb⁻¹ [93] is slightly stronger than corresponding ATLAS analysis with 139 fb⁻¹ data [94] in limiting the electroweakinos when $\mu \lesssim 300$ GeV.

¹⁴ $R \equiv s/s_95^{\text{obs}}$ is the ratio of theoretical prediction of the signal to its experimental observed 95% C.L. upper limit; therefore, $R > 1$ indicates that the theoretical prediction contradicts experimental observation. For more details about the calculation of R , see our previous works [35,44].

A_{λ_ν} , and $m_{\tilde{\nu}}$. Especially, the constraints are rather weak for Region I when $2\kappa/\lambda > 1$ and the coannihilation is responsible for the relic density.

- (ii) For both Regions I and II, $2\kappa/\lambda$ may be less than 1. This situation is quite similar to that of Region III where $\tilde{\chi}_1^0$ is Singlino dominated and λ_ν must be larger than 0.1 to get right relic density. Then from our previous discussion about Regions I and II, one can infer that Region I has been tightly limited by DM DD experiments, while Region II is still allowed. We checked the correctness of this conclusion. Moreover, the best way to detect the Higgsinos is through the process $pp \rightarrow \tilde{\chi}_{2,3}\tilde{\chi}_1^\pm \rightarrow Z^{(*)}W^{(*)}2\tilde{\chi}_1^0$, and the trilepton signal is usually suppressed due to the open up of the decay channels $\tilde{\chi}_{2,3}^0 \rightarrow h_1\tilde{\chi}_1^0, h_2\tilde{\chi}_1^0, A_1\tilde{\chi}_1^0$. As a result, the samples in these regions may escape the LHC constraint.

In Table V, we summarize the DM physics and the LHC signal of the three regions, which may serve as a guideline to pick out good explanations of the excesses. We also choose a benchmark point for the setting in Table II, which sets $\lambda_\nu = 0.045$, $A_{\lambda_\nu} = -201.8$ GeV, $m_{\tilde{\nu}} = 133.7$ GeV, and consequently predicts $\Omega h^2 = 0.1243$ and $\sigma_{\tilde{\nu}_1-p}^{\text{SI}} = 1.6 \times 10^{-47}$ cm². We calculate its theoretical fine-tunings in predicting some measurements and get $\Delta_Z = 6.37$, $\Delta_{m_{h_1}} = 12.95$, $\Delta_{m_{h_2}} = 62.2$, $\Delta_{\Omega h^2} = 20.2$, $\Delta_{\sigma_{\tilde{\nu}_1-p}^{\text{SI}}} = 8.58$, $\Delta_{\mu_{\text{CMS}}} = 6.16$, and $\Delta_{\mu_{\text{LEP}}} = 20.65$. In the calculation, we adopt the definition of Δ_Z and Δ_{h_i} ($i=1, 2, 3$) from [95,96], respectively, with the input parameters defined at the electroweak scale. As for the last four fine-tunings, they are obtained by maximizing the ratio $\partial \ln O / \partial \ln p_i$ over the input parameter p_i in Eqs. (3.1) and (4.1) with O denoting an observable. These results indicate that the explanation of the excesses in the seesaw extension is quite natural and thus deserves a careful study.

V. CONCLUSIONS

The discovery of the SM-like Higgs boson at the LHC validates the Higgs mechanism, while the deficiencies in the Higgs sector of the SM imply a more complex structure to account for the EWSB. The long-standing $b\bar{b}$ excess at LEP-II and the continuously observed $\gamma\gamma$ excess by CMS Collaboration provide potentially useful hints about the EWSB, and thus they deserve a careful study in new physics models.

In this work, we show by both analytic formulas and numerical results that the NMSSM with the Type-I seesaw mechanism can naturally predict the central values of the excesses in certain corners of its parameter space, which are categorized into three regions, and the explanations are consistent with the Higgs data of the discovered Higgs boson, B -physics, and DM physics measurements, the

electroweak precision data, as well as the LHC search for sparticles. This great capability of the theory basically comes from the relaxation of the DM DD constraints. Explicitly speaking, the seesaw mechanism augments the NMSSM by three generations of right-handed neutrino fields and renders the right-handed sneutrino as a viable DM candidate. Due to the gauge singlet nature of the DM, its scattering with nucleon is suppressed in most cases to coincide spontaneously with the latest XENON-1T results. Consequently, broad parameter spaces in the Higgs sector, especially a light Higgsino mass, are resurrected as experimentally allowed, which makes the theory well suited to explain the excesses.

Our results indicate that the scalar responsible for the excesses should contain a sizable component of the SM Higgs field, and its decay branching ratio into $\gamma\gamma$ state is preferred several times larger than corresponding SM prediction to account for the excesses. The latter can be achieved by a moderately suppressed coupling of the scalar with bottom quarks (in comparison with its other Yukawa couplings) and meanwhile a significant enhancement of its coupling with photons (the chargino-mediated loops play a role in such a process). Correspondingly, the couplings of the SM-like Higgs boson deviate from their SM predictions at a level of 10%. If the excesses are corroborated in future, these predictions will serve as the criteria to testify the theory by the precise determination of the scalars' property at next generation e^+e^- colliders [17]. Our results also indicate that the explanations are distributed in three isolated parameter regions with different features. These regions can be further classified into five cases according to their underlying DM physics and the LHC signal, which are summarized in Table V. The first case in the table is least constrained by current measurements in DM physics and the sparticle search at the LHC, while the second case has been tightly limited by the XENON-1T experiment. The Higgsinos in these cases can survive the LHC constraints by any of the following mechanism: the compressed mass spectrum of the Higgsinos with the sneutrino DM, heavy Higgsinos, or the suppression of $\text{Br}(\tilde{\chi}_{2,3}^0 \rightarrow Z\tilde{\chi}_1^0)$. We remind that part of the regions will be explored by updated DM DD experiments and the SUSY search at the LHC, and once new exotic signals are discovered, they will provide complementary information about the EWSB. We also remind that the strong constraints of the XENON-1T experiment on the second case may be avoided in the NMSSM with the inverse seesaw mechanism [46]. The DM physics of this extension is somewhat similar to that of the Type-I extension except that it corresponds to a much more complicated sneutrino sector with several additional parameters and thus predicts more flexible DM physics.

ACKNOWLEDGMENTS

This work was supported by the National Natural Science Foundation of China under Grant No. 11575053.

- [1] G. Aad *et al.* (ATLAS Collaboration), *Phys. Lett. B* **716**, 1 (2012).
- [2] S. Chatrchyan *et al.* (CMS Collaboration), *Phys. Lett. B* **716**, 30 (2012).
- [3] ATLAS Collaboration, CERN Report No. ATLAS-CONF-2019-005, 2019.
- [4] R. Barate *et al.* (LEP Working Group for Higgs boson searches, ALEPH, DELPHI, L3, OPAL Collaborations), *Phys. Lett. B* **565**, 61 (2003).
- [5] S. Schael *et al.* (ALEPH, DELPHI, L3, OPAL, LEP Working Group for Higgs Boson Searches Collaborations), *Eur. Phys. J. C* **47**, 547 (2006).
- [6] A. M. Sirunyan *et al.* (CMS Collaboration), *Phys. Lett. B* **793**, 320 (2019).
- [7] CMS Collaboration, CERN Tech. Report No. CMS-PAS-HIG-14-037, 2015.
- [8] ATLAS Collaboration, CERN Report No. ATLAS-CONF-2018-025, 2018.
- [9] S. Heinemeyer and T. Stefaniak, *Proc. Sci., CHARGED2018* (2019) 016 [arXiv:1812.05864].
- [10] J. Cao, X. Guo, Y. He, P. Wu, and Y. Zhang, *Phys. Rev. D* **95**, 116001 (2017).
- [11] F. Richard, arXiv:1712.06410.
- [12] D. Sachdeva and S. Sadhukhan, arXiv:1908.01668.
- [13] P. J. Fox and N. Weiner, *J. High Energy Phys.* **08** (2018) 025.
- [14] P. Mondal, S. Maharana, and A. Kundu, arXiv:1907.12808.
- [15] U. Haisch and A. Malinauskas, *J. High Energy Phys.* **03** (2018) 135.
- [16] T. Biekotter, M. Chakraborti, and S. Heinemeyer, *Proc. Sci., CORFU2018* (2019) 015 [arXiv:1905.03280].
- [17] T. Biekotter, M. Chakraborti, and S. Heinemeyer, *Eur. Phys. J. C* **80**, 2 (2020).
- [18] W. G. Hollik, S. Liebler, G. Moortgat-Pick, and S. Paßehr, and G. Weiglein, *Eur. Phys. J. C* **79**, 75 (2019).
- [19] F. Domingo, S. Heinemeyer, and S. Paßehr, and G. Weiglein, *Eur. Phys. J. C* **78**, 942 (2018).
- [20] J. Q. Tao *et al.*, *Chin. Phys. C* **42**, 103107 (2018).
- [21] C. Beskidt, W. de Boer, and D. I. Kazakov, *Phys. Lett. B* **782**, 69 (2018).
- [22] K. Choi, S. H. Im, K. S. Jeong, and C. B. Park, *Eur. Phys. J. C* **79**, 956 (2019).
- [23] T. Biekotter, S. Heinemeyer, and C. Munoz, *Eur. Phys. J. C* **78**, 504 (2018).
- [24] T. Biekotter, S. Heinemeyer, and C. Munoz, *Eur. Phys. J. C* **79**, 667 (2019).
- [25] U. Ellwanger, C. Hugonie, and A. M. Teixeira, *Phys. Rep.* **496**, 1 (2010).
- [26] U. Ellwanger and A. M. Teixeira, *J. High Energy Phys.* **10** (2014) 113.
- [27] J. S. Kim, D. Schmeier, and J. Tattersall, *Phys. Rev. D* **93**, 055018 (2016).
- [28] J. Cao, Y. He, L. Shang, W. Su, and Y. Zhang, *J. High Energy Phys.* **08** (2016) 037.
- [29] U. Ellwanger and C. Hugonie, *Eur. Phys. J. C* **78**, 735 (2018).
- [30] U. Ellwanger, *J. High Energy Phys.* **03** (2012) 044.
- [31] J. J. Cao, Z. X. Heng, J. M. Yang, Y. M. Zhang, and J. Y. Zhu, *J. High Energy Phys.* **03** (2012) 086.
- [32] M. Badziak, M. Olechowski, and S. Pokorski, *J. High Energy Phys.* **06** (2013) 043.
- [33] J. Cao, F. Ding, C. Han, J. M. Yang, and J. Zhu, *J. High Energy Phys.* **11** (2013) 018.
- [34] K. S. Jeong, Y. Shoji, and M. Yamaguchi, *J. High Energy Phys.* **11** (2014) 148.
- [35] J. Cao, Y. He, L. Shang, Y. Zhang, and P. Zhu, *Phys. Rev. D* **99**, 075020 (2019).
- [36] J. Cao, L. Shang, P. Wu, J. M. Yang, and Y. Zhang, *J. High Energy Phys.* **10** (2015) 030.
- [37] N. Aghanim *et al.* (Planck Collaboration), arXiv:1807.06209.
- [38] J. Cao, L. Shang, P. Wu, J. M. Yang, and Y. Zhang, *Phys. Rev. D* **91**, 055005 (2015).
- [39] E. Aprile *et al.* (XENON Collaboration), *Phys. Rev. Lett.* **121**, 111302 (2018).
- [40] E. Aprile *et al.* (XENON Collaboration), *Phys. Rev. Lett.* **122**, 141301 (2019).
- [41] J. Cao, Y. He, L. Shang, W. Su, P. Wu, and Y. Zhang, *J. High Energy Phys.* **10** (2016) 136.
- [42] M. Badziak, M. Olechowski, and P. Szczerbiak, *J. High Energy Phys.* **03** (2016) 179.
- [43] J. Cao, X. Guo, Y. He, L. Shang, and Y. Yue, *J. High Energy Phys.* **10** (2017) 044.
- [44] J. Cao, J. Li, Y. Pan, L. Shang, Y. Yue, and D. Zhang, *Phys. Rev. D* **99**, 115033 (2019).
- [45] J. Cao, Y. He, L. Meng, Y. Pan, Y. Yue, and P. Zhu, arXiv:1903.01124.
- [46] J. Cao, L. Meng, Y. Yue, H. Zhou, and P. Zhu, arXiv:1910.14317.
- [47] M. J. Baker *et al.*, *J. High Energy Phys.* **12** (2015) 120.
- [48] K. Griest and D. Seckel, *Phys. Rev. D* **43**, 3191 (1991).
- [49] D. G. Cerdeno, C. Munoz, and O. Seto, *Phys. Rev. D* **79**, 023510 (2009).
- [50] D. G. Cerdeno and O. Seto, *J. Cosmol. Astropart. Phys.* **08** (2009) 032.
- [51] S. F. King, M. Muhlleitner, R. Nevzorov, and K. Walz, *Nucl. Phys.* **B870**, 323 (2013).
- [52] E. Bagnaschi *et al.*, *Eur. Phys. J. C* **78**, 256 (2018).
- [53] R. Kitano and K. y. Oda, *Phys. Rev. D* **61**, 113001 (2000).
- [54] M. Tanabashi *et al.* (Particle Data Group), *Phys. Rev. D* **98**, 030001 (2018).
- [55] J. A. Casas and A. Ibarra, *Nucl. Phys.* **B618**, 171 (2001).
- [56] G. Aad *et al.* (ATLAS Collaboration), arXiv:1908.08215.
- [57] G. Aad *et al.* (ATLAS Collaboration), arXiv:1911.06660.
- [58] G. Aad *et al.* (ATLAS Collaboration), arXiv:1911.12606.
- [59] A. M. Sirunyan *et al.* (CMS Collaboration), arXiv:1910.01185.
- [60] S. Heinemeyer *et al.* (LHC Higgs Cross Section Working Group Collaboration), arXiv:1307.1347.
- [61] K. Choi, S. H. Im, K. S. Jeong, and M. Yamaguchi, *J. High Energy Phys.* **02** (2013) 090.
- [62] U. Ellwanger, *Phys. Lett. B* **698**, 293 (2011).
- [63] J. Cao, Z. Heng, T. Liu, and J. M. Yang, *Phys. Lett. B* **703**, 462 (2011).
- [64] F. Staub, *Comput. Phys. Commun.* **185**, 1773 (2014).
- [65] F. Staub, *Comput. Phys. Commun.* **184**, 1792 (2013).
- [66] F. Staub, arXiv:0806.0538.
- [67] W. Porod and F. Staub, *Comput. Phys. Commun.* **183**, 2458 (2012).
- [68] W. Porod, F. Staub, and A. Vicente, *Eur. Phys. J. C* **74**, 2992 (2014).

- [69] P. Bechtle, S. Heinemeyer, O. Stal, T. Stefaniak, and G. Weiglein, *Eur. Phys. J. C* **75**, 421 (2015).
- [70] P. Bechtle, S. Heinemeyer, O. Stål, T. Stefaniak, and G. Weiglein, *J. High Energy Phys.* **11** (2014) 039.
- [71] G. Belanger, F. Boudjema, A. Pukhov, and A. Semenov, *Comput. Phys. Commun.* **185**, 960 (2014).
- [72] D. Barducci, G. Belanger, J. Bernon, F. Boudjema, J. Da Silva, S. Kraml, U. Laa, and A. Pukhov, [arXiv:1606.03834](https://arxiv.org/abs/1606.03834).
- [73] G. Belanger, F. Boudjema, C. Hugonie, A. Pukhov, and A. Semenov, *J. Cosmol. Astropart. Phys.* **09** (2005) 001.
- [74] F. Feroz, M. P. Hobson, and M. Bridges, *Mon. Not. R. Astron. Soc.* **398**, 1601 (2009).
- [75] F. Feroz, M. P. Hobson, E. Cameron, and A. N. Pettitt, [arXiv:1306.2144](https://arxiv.org/abs/1306.2144).
- [76] M. Tanabashi *et al.* (Particle Data Group), *Phys. Rev. D* **98**, 030001 (2018).
- [77] G. Altarelli and R. Barbieri, *Phys. Lett. B* **253**, 161 (1991).
- [78] G. Altarelli, R. Barbieri, and S. Jadach, *Nucl. Phys.* **B369**, 3 (1992); **B376**, 444(E) (1992).
- [79] G. Altarelli, R. Barbieri, and F. Caravaglios, *Phys. Lett. B* **349**, 145 (1995).
- [80] M. E. Peskin and T. Takeuchi, *Phys. Rev. Lett.* **65**, 964 (1990).
- [81] M. E. Peskin and T. Takeuchi, *Phys. Rev. D* **46**, 381 (1992).
- [82] J. Cao and J. M. Yang, *J. High Energy Phys.* **12** (2008) 006.
- [83] J. de Blas, M. Ciuchini, E. Franco, S. Mishima, M. Pierini, L. Reina, and L. Silvestrini, *J. High Energy Phys.* **12** (2016) 135.
- [84] D. J. Miller, R. Nevzorov, and P. M. Zerwas, *Nucl. Phys.* **B681**, 3 (2004).
- [85] U. Ellwanger, J. F. Gunion, and C. Hugonie, *J. High Energy Phys.* **02** (2005) 066.
- [86] U. Ellwanger and C. Hugonie, *Comput. Phys. Commun.* **175**, 290 (2006).
- [87] A. Fowlie and M. H. Bardsley, *Eur. Phys. J. Plus* **131**, 391 (2016).
- [88] S. Chang, R. Edezhath, J. Hutchinson, and M. Luty, *Phys. Rev. D* **89**, 015011 (2014).
- [89] A. Berlin, D. Hooper, and S. D. McDermott, *Phys. Rev. D* **89**, 115022 (2014).
- [90] J. Alwall, R. Frederix, S. Frixione, V. Hirschi, F. Maltoni, O. Mattelaer, H.-S. Shao, T. Stelzer, P. Torrielli, and M. Zaro, *J. High Energy Phys.* **07** (2014) 079.
- [91] J. Alwall, M. Herquet, F. Maltoni, O. Mattelaer, and T. Stelzer, *J. High Energy Phys.* **06** (2011) 128.
- [92] M. Aaboud *et al.* (ATLAS Collaboration), *J. High Energy Phys.* **10** (2018) 180.
- [93] A. M. Sirunyan *et al.* (CMS Collaboration), *J. High Energy Phys.* **03** (2018) 166.
- [94] For ATLAS analyses on supersymmetry search at the LHC, <https://atlas.web.cern.ch/Atlas/GROUPS/PHYSICS/CombinedSummaryPlots/SUSY/>.
- [95] U. Ellwanger, G. Espitalier-Noel, and C. Hugonie, *J. High Energy Phys.* **09** (2011) 105.
- [96] M. Farina, M. Perelstein, and B. Shakya, *J. High Energy Phys.* **04** (2014) 108.